ANL-ART-176
ANL-METL-18

Thermal Hydraulic Experimental Test Article – Status Report for FY2019

Nuclear Sciences and Engineering Division

About Argonne National Laboratory

Argonne is a U.S. Department of Energy laboratory managed by UChicago Argonne, LLC under contract DE-AC02-06CH11357. The Laboratory's main facility is outside Chicago, at 9700 South Cass Avenue, Argonne, Illinois 60439. For information about Argonne
and its pioneering science and technology programs, see www.anl.gov.

ANL-ART-176
ANL-METL-18

Thermal Hydraulic Experimental Test Article – Status Report for FY2019

M. Weathered, D. Kultgen, E. Kent, C. Grandy, T. Sumner

Nuclear Sciences and Engineering Division
Argonne National Laboratory

August 2019

TABLE OF CONTENTS

LIST OF FIGURES

LIST OF TABLES

1. Executive Summary

The Thermal Hydraulic Experimental Test Article (THETA) is a facility that will be used to develop sodium components and instrumentation as well as acquire experimental data for validation of reactor thermal hydraulic and safety analysis codes. The facility will simulate nominal conditions as well as protected/unprotected loss of flow accidents in an SFR. High fidelity distributed temperature profiles of the developed flow field will be acquired with Rayleigh backscatter based optical fiber temperature sensors. The facility is being designed in partnership with systems code experts to tailor the experiment to ensure the most relevant and highest quality data for code validation.

Figure 1 illustrates the main components of the primary system. THETA will be installed in the Mechanisms Engineering Test Loop (METL) with the primary system in the 28 inch Test Vessel #4, the secondary system in the 18-inch Test Vessel #6, and its sodium-to-air heat exchanger will occupy the location for 18-inch Test Vessel #5 (Test Vessel #5 will not be installed), Figure 2.

The design work for the facility has been completed and is currently in the procurement, manufacturing and initial testing stage. The THETA primary system, including the redan, inlet and outlet plenum, 38 kW electric core simulant heater, submerged flowmeter, pump, and all instrumentation has either been procured or is currently being tested at Argonne. The secondary sodium system for cooling the tube-side sodium of the intermediate heat exchanger has all been analyzed according to ASME code and is in the final development stages before procurement.

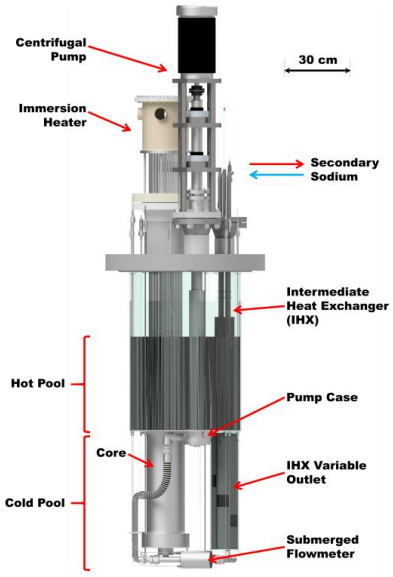

Figure 1 – THETA Primary Heat Transport System (28 inch test vessel not shown)

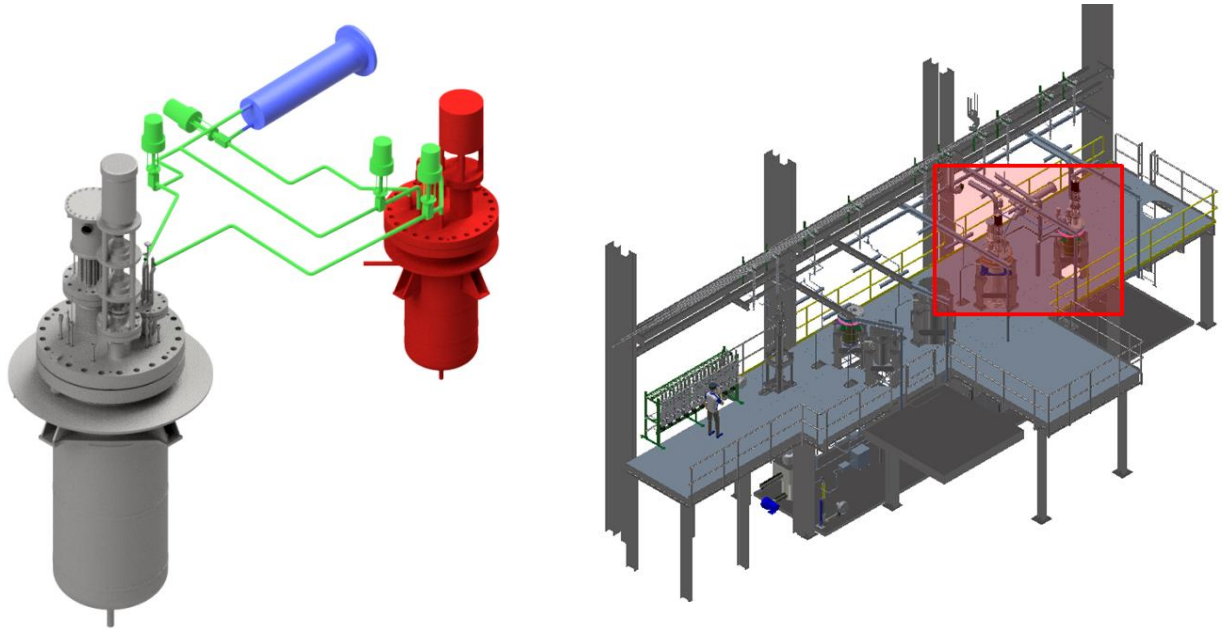

Figure 2: Isometric drawing of THETA primary vessel (gray), secondary vessel (red), AHX (blue), and inter-vessel piping/valves (green), left. Location of THETA in METL facility highlighted with red square, right.

2. Introduction

The Thermal Hydraulic Experimental Test Article (THETA) is a METL vessel experiment designed for testing and validating sodium fast reactor components and phenomena. THETA has been scaled using a non-dimensional Richardson number approach to represent temperature distributions during nominal and loss of flow conditions in a sodium fast reactor (SFR). The facility is being constructed with versatility in mind, allowing for the installation of various immersion heaters, heat pipes, and heat exchangers without significant facility modification. THETA is being designed in collaboration with systems code experts to inform the geometry and sensor placement to acquire the highest value code validation data.

2.1. Scaling Approach

In order to scale an experimental facility, it is important to analyze the relevant non-dimensional numbers. It has been shown in literature that the Richardson number predicts the temperature distribution in a large stratified body of fluid such as the hot pool of a sodium fast reactor, Eq. 1 [1]–[4]:

$$Ri = \frac{Buoyancy}{Inertial} = \frac{Gr}{Re^2} = \frac{\beta \Delta T g D_h}{U^2} \quad (1)$$

Where β is the fluid's coefficient of thermal expansion, ΔT is the temperature differential of the pool, g is gravitational acceleration, D_h is the effective diameter, and U is the effective axial cross sectional velocity between the UIS and the redan.

The characteristic length for the Richardson number is typically taken as the effective diameter of the plenum (the annulus between the UIS and the redan) [2]. The effective diameter, or hydraulic diameter, is found using Eq. 2.

$$D_h = \frac{4 * cross\ sectional\ area}{wetted\ perimeter} = \frac{\left({D_r}^2 - {D_{UIS}}^2\right)}{D_r + D_{UIS}} \quad (2)$$

Where D_r is the redan inner diameter and D_{UIS} is the upper internal structure diameter. An upper internal structure is a typical feature of an SFR and it usually takes the form of a cylinder positioned concentric to the upper plenum, above the core. Instrumentation, control rods, and fuel handling devices are located within this upper internal structure. Its presence above the core greatly affects the stratification behavior of the upper plenum as it is positioned immediately above the core outlet and serves to impinge and redistribute axial flow up the redan.

During an SFR accident with loss of primary pump power, the pumps are designed to coast down via inertial forces before stopping. During this time the primary convective heat transport mechanism to cool the reactor core switches from forced pump flow convection to natural convection driven by density differences in the non-isothermal sodium. In this reactor condition the Richardson number is greatest and thus thermal stratification is most likely. Ieda performed a review of various stratification studies and found a threshold value of Ri = 2,000, above which, significant thermal stratification begins to occur in the upper plenum of a reactor, Figure 3 [2]. This stratification can cause great thermal stress on the redan and pressure vessel as well as uncertainty in the thermal hydraulic parameters required to design a satisfactory reactor decay heat system (e.g. primary inlet temperature DRACS). Table 1 summarizes some historical thermal stratification experiments; 1-to-1 similitude was maintained with the Richardson number between the model and actual reactor for all of these works.

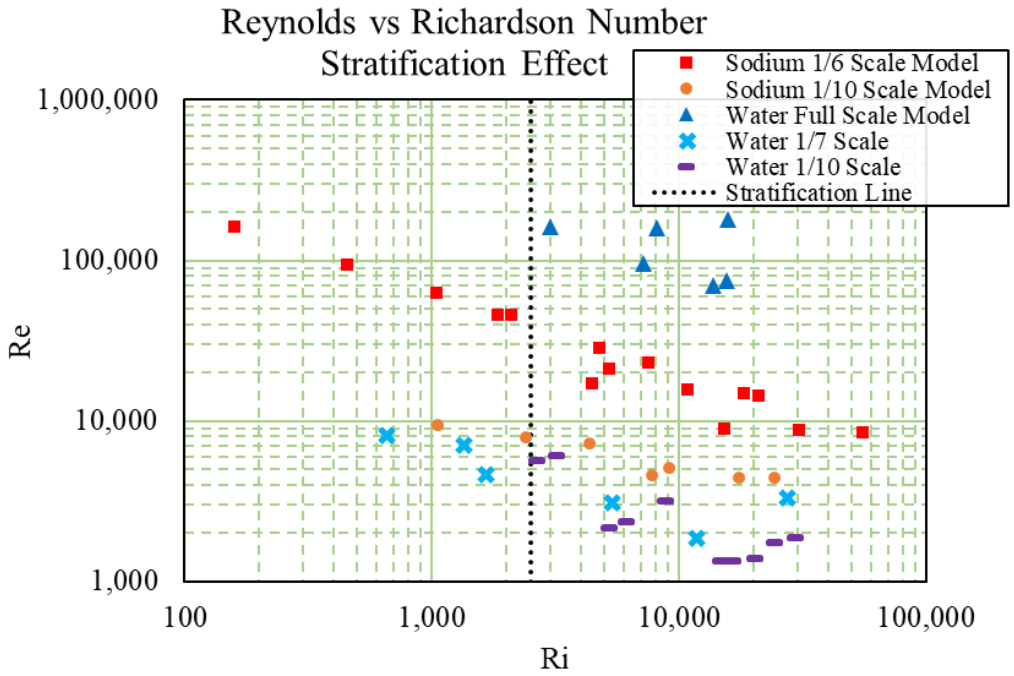

Figure 3: Threshold of stratification occurrence in experimental studies of reactor upper plenums. Plot adapted from [2]

Table 1: Summary of scaling parameters from some previous stratifications experiments from literature [2]**. Note that the asterisk defines the non-dimensional number as a ratio between the model and the actual reactor parameters.**

Experiment #	Fluid	Scale	Ri*	Pe*	Re*
1	Na	1/6	1	0.07	0.09
2	Na	1/10	1	0.02	0.025
3	Na	1/10	1	-	-
4	H_2O	1/3	1	500	0.7
5	H_2O	1/6	1	-	-
6	H_2O	1/7	1	-	-
7	H_2O	1/10	1	6	-

In order to scale an experiment to model the thermal hydraulic behaviors of a typical SFR, the Richardson number should scale with one-to-one similitude, as seen in Table 1. During an unprotected loss of flow accident (ULOF), core outlet temperature quickly rises without a successful SCRAM of control rods and coolant flowrate drops as the pump spins down. Using parameters from the Advanced Burner Test Reactor (ABTR) during a ULOF, Figure 4 [5], we may propose nominal thermal hydraulic design parameters for THETA, Table 2.

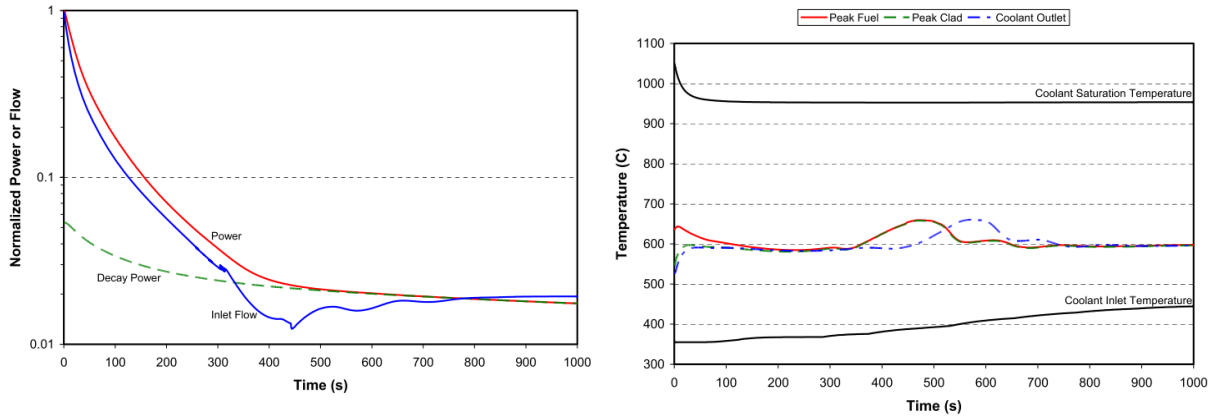

Figure 4: ABTR ULOF Transient Total Power and Channel 5 Flow, left. ABTR ULOF Transient Temperatures for Channel 5, right. [5]

Table 2: Comparison of parameters for Argonne National Laboratory's Advanced Burner Test Reactor (ABTR) and the proposed scaled reactor experiment Thermal Hydraulic Experimental Test Article (THETA). Note that parameters for ABTR were taken during 20% of nominal flow during a loss of flow incident. Volumetric thermal expansion (β) and density (ρ) taken from Fink and Leibowitz for sodium at 800 K [6]

Parameter:	ABTR	THETA
β	2.82E-4 [K^{-1}]	2.82E-4 [K^{-1}]
ρ	828.4 [kg/m^3]	828.4 [kg/m^3]
D_{UIS}	1.3 [m]	0.20 [m]
D_r	4.9 [m]	0.64 [m]
D_h	3.61 [m]	0.43 [m]
Flowrate	7.57E-2 [m^3/s]	3.15E-4 [m^3/s]
	(=1200 [GPM])	*(=5 [GPM])*
U	*4.3E-3 [m/s]*	*1.1E-3 [m/s]*
ΔT	90 [°C]	50 [°C]
Ri	48,450 [-]	48,562 [-]
Re	42,864 [-]	1,323 [-]

As one can see the Richardson number may be matched with one-to-one similitude with reasonable experimental thermal hydraulic parameters. In Table 2 the Reynolds number for THETA is not fully turbulent, a flow rate of approximately 19 GPM produces Re > 5,000 – a flow rate well within the current primary pump curves, as will be introduced in a future section (Figure 38). Thus, the effect of turbulence on the characteristics of thermal stratification may be studied.

2.2. System Overview and Systems Code Application

THETA possesses all the major thermal hydraulic components of a pool type sodium cooled reactor. A P&ID has been included in Figure 5 showing the primary and secondary sodium circuit. A cross section of the primary vessel shows pool and core geometry, Figure 6. As can be seen, a 28" METL vessel is used for the primary sodium circuit and an 18" METL vessel is used for the secondary sodium cooling system. An isometric model of the primary/secondary vessels, inter-vessel piping, and air-to-sodium heat exchanger (AHX) can be found in Figure 2.

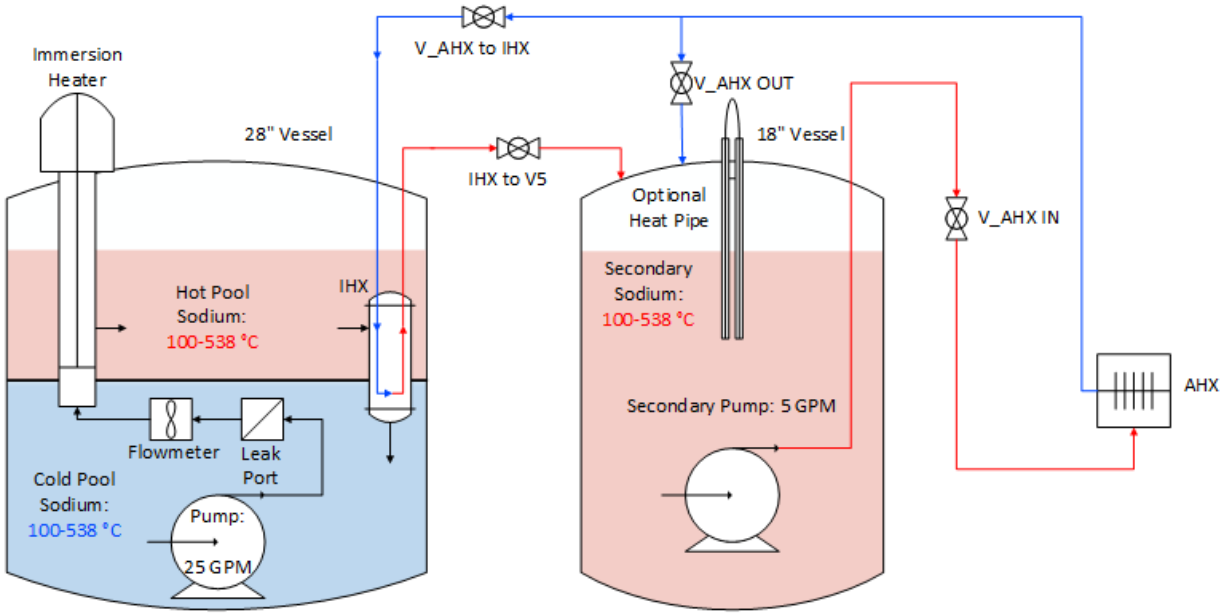

Figure 5: P&ID schematic of THETA

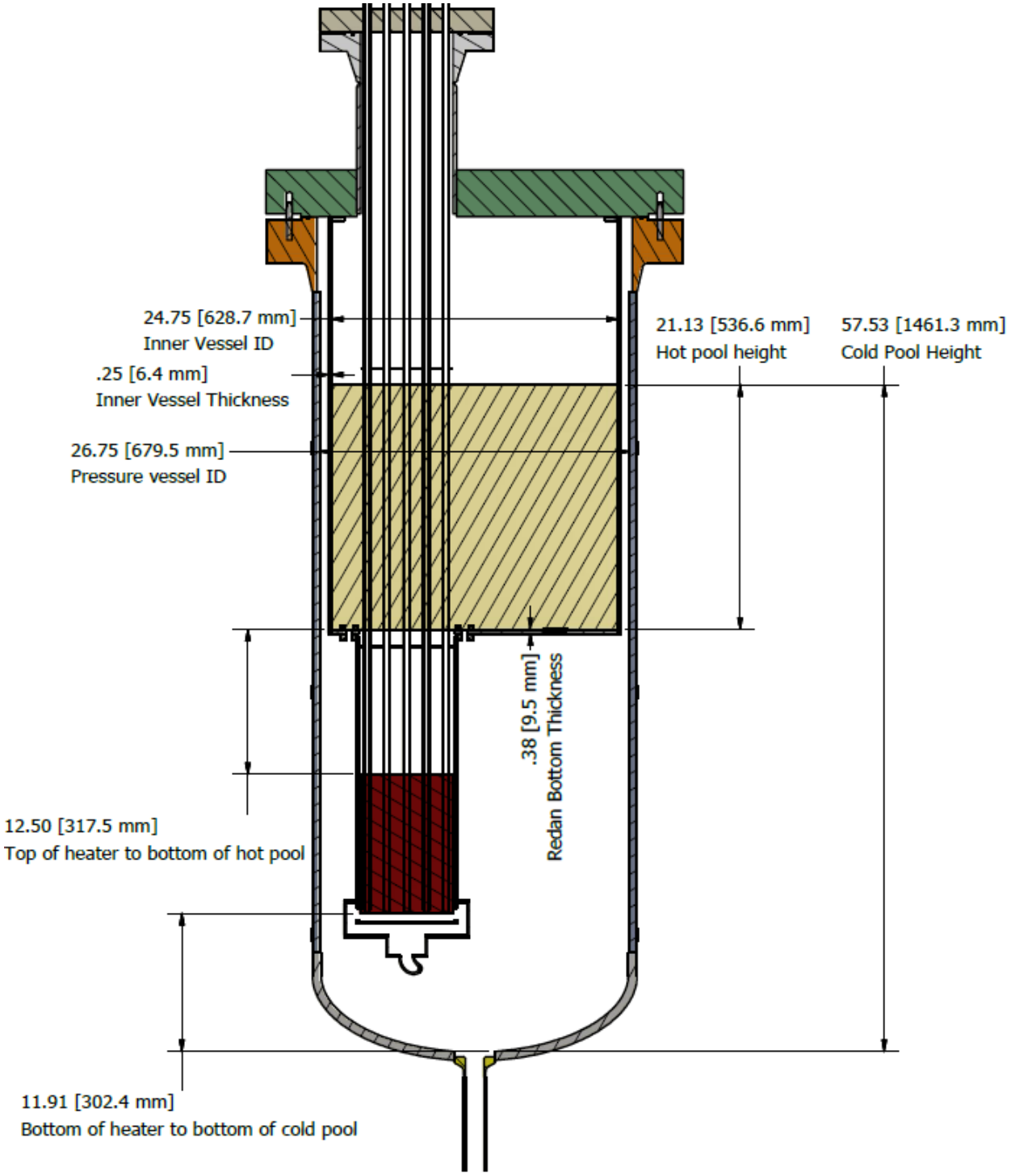

Figure 6: THETA pool and core geometry. Core nominal diameter: 0.2 [m] (8”), core heated length: 0.3 [m] (12”) see heater geometry in Figure 41 for more information

THETA will be located on the METL mezzanine, in 28” and 18” nominal OD vessels, Figure 7

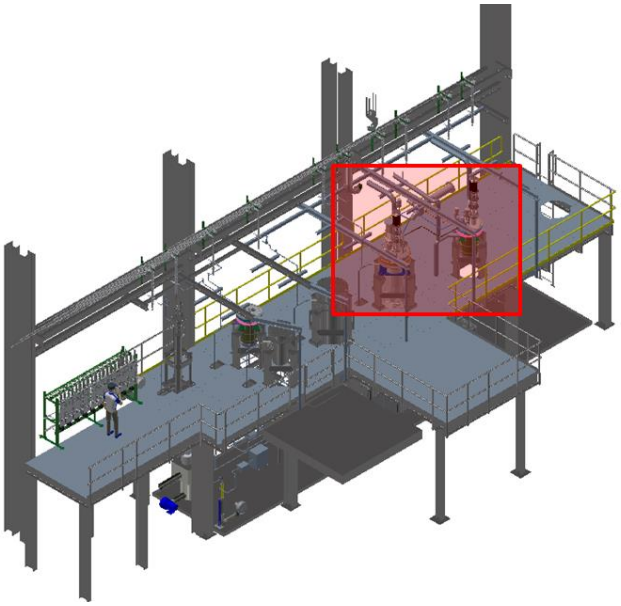

Figure 7: Location of THETA on METL mezzanine

Argonne National Laboratory's SAS4A/SASSYS-1 computer code is used for thermal hydraulic and safety analysis of power and flow transients in liquid metal cooled reactors. Figure 8 gives a graphic displaying the segments and compressible volumes used to perform the deterministic analysis of anticipated events such as protected/un-protected loss of flow reactor trips etc. While SAS4A/SASSYS-1 was benchmarked against tests in historic reactors, such as EBR-II [7], a modern liquid metal thermal hydraulic facility is required for further system's code validation.

A parameter of interest is the differential in elevation between the intermediate heat exchanger (IHX) outlet and the core outlet. This differential will dictate the thermal stratification in the cold pool, thus driving the development of particular natural convection phenomena during reactor trips. The natural convection phenomena in the cold pool can then affect the thermal stratification in the reactor hot pool as sodium temperature from compressible volumes (CV) 3-5 (cold pool) will be transmitted to CV 1-2 (hot pool) in the SAS4A/SASSYS-1 computer code.

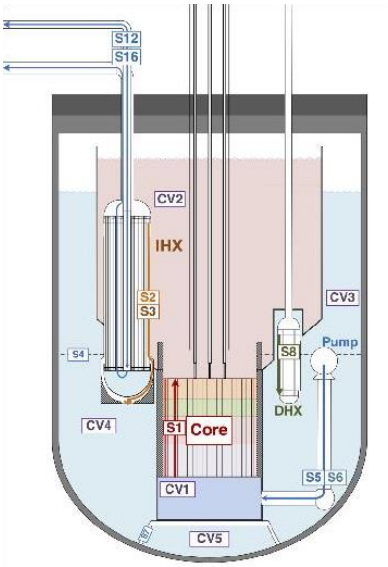

Figure 8: Schematic of SAS4A/SASSYS-1 showing locations of various compressible volumes (CV#) and segments (S#)

3. Primary Vessel Component Summary

The following section presents a summary of all primary vessel components as of August 2019, Figure 9. Currently all components have been received, are being manufactured or final design drawings are being sent in for manufacture.

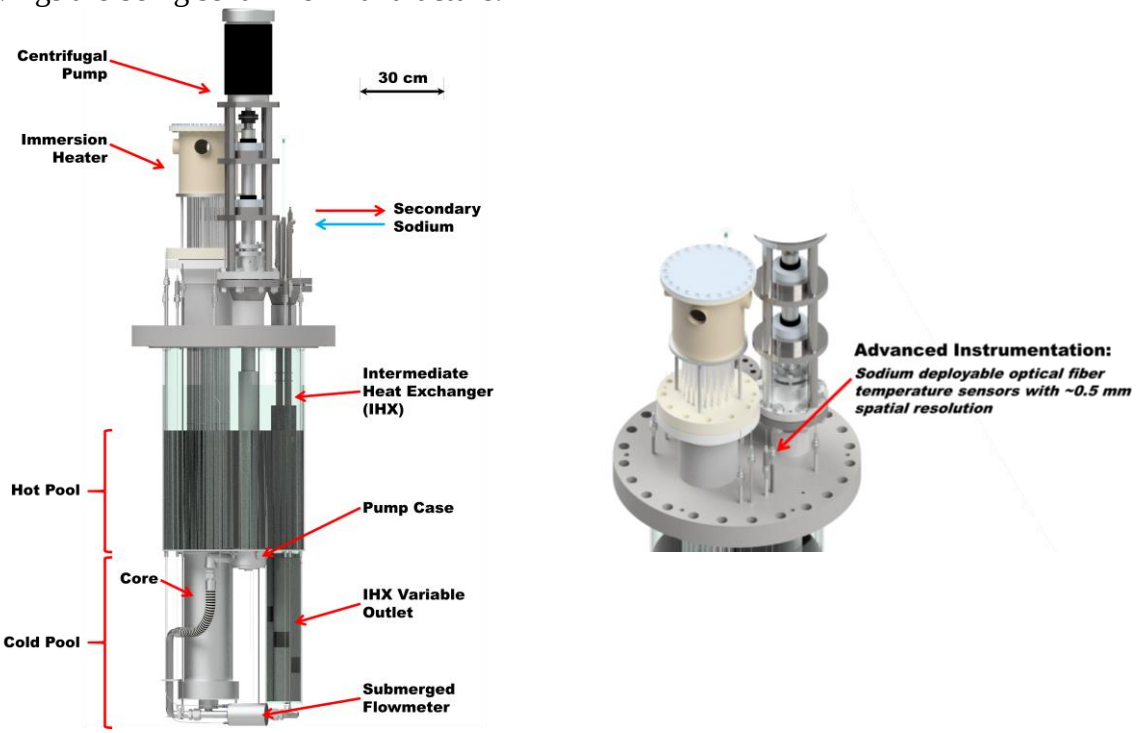

Figure 9: THETA primary vessel components

3.1. Instrumentation

Table 3 summarizes THETA instrumentation which includes single and multi-point thermocouples, distributed optical fiber temperature sensors, and flowmeter voltage measurements. The port locations on the top flange have been labeled in Figure 10.

Table 3: THETA instrumentation and measurement. Port positions provided in Figure 10

Port #	Instrument	Measurement
1	Single TC	Heater inlet temperature
2	Single TC	Heater outlet temperature
3	Fiber	Hot and cold pool temperature
4	Rake TC	Hot and cold pool temperature
5	Rake TC	IHX outlet temperatures
6	Rake TC	Hot and cold pool temperature
7	Fiber	Hot and cold pool temperature
8	Rake TC	Outside inner vessel cold pool temperature
9	Rake TC	Hot and cold pool temperature
10	Fiber	Hot and cold pool temperature
11	MI Cable	Flowmeter voltage
12	Single TC	Flowmeter temperature
13	Fiber	Hot and cold pool temperature
14	Fiber	IHX temperature
15	Rake TC	IHX temperature
16-20	Single TCs	Heater temperatures, 3” above inlet

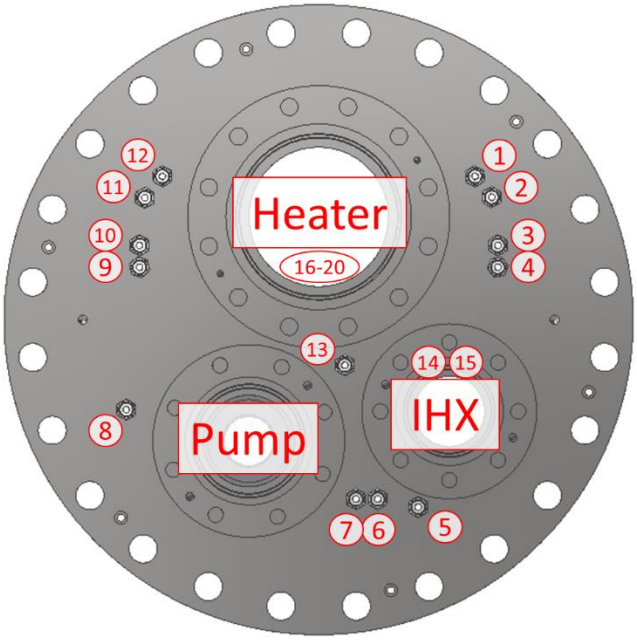

Figure 10: THETA instrumentation port locations

Port # 4, 6, and 9 possess 1/4" OD, 25 junction, k-type ungrounded thermocouple probes. The junctions possess a pitch of 2.375" and capture hot and cold pool axial temperatures with high fidelity, Figure 11. All thermocouple probes will be x-rayed to ensure a tight spatial tolerance of ±1/16".

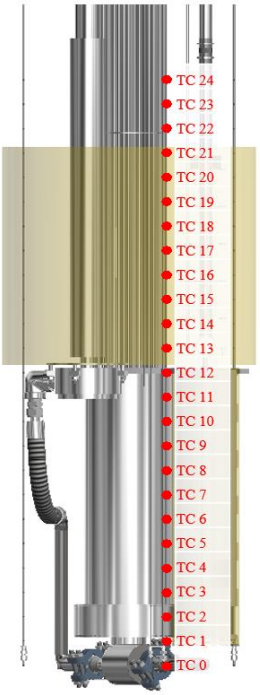

Figure 11: Multipoint TC positions for ports 4, 6, and 9

Optical fiber temperature sensors will be used to acquire distributed temperature data at spatial resolutions down to 0.65 mm and measurement rates of up to 250 Hz. These sensors are constructed from single mode silica fibers, Figure 12. An ODISI 6104 optical fiber interrogator system has been purchased and received from Luna Innovations, manufacturer specifications provided in Table 4.

.

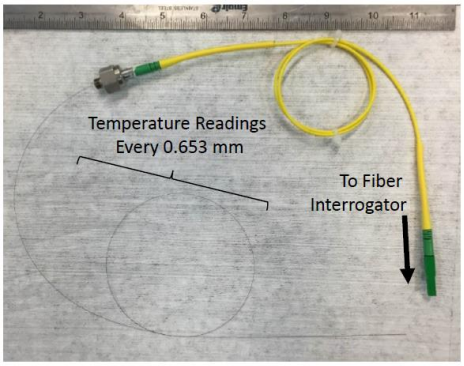

Figure 12: Photo showing 150 µm OD silica optical fiber

Table 4: ODISI 6104 spatial resolution and measurement rate

Spatial Resolution [mm]	Measurement Rate [Hz]
0.65	62.5
1.3	125
2.6	250

Optical fibers will be sheathed in a protective 1/16” OD 0.009” wall, 316 stainless steel capillary tube to protect them from sodium. Given there are no connection points for the 1/16” capillaries at the base of the 28” METL vessel, the optical fiber capillaries in ports 3, 7, and 10 will be mechanically attached to 1/4” multipoint thermocouple probes in ports 4, 6, and 9 to provide support, Figure 13 and Figure 14.

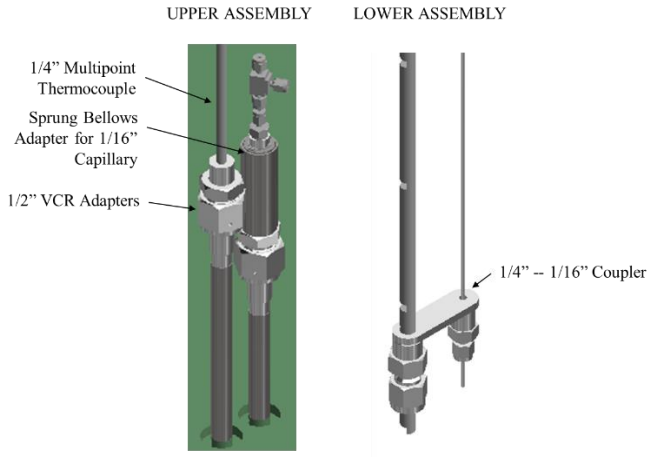

Figure 13: Optical fiber capillaries mechanically coupled to 1/4" multi-junction thermocouples

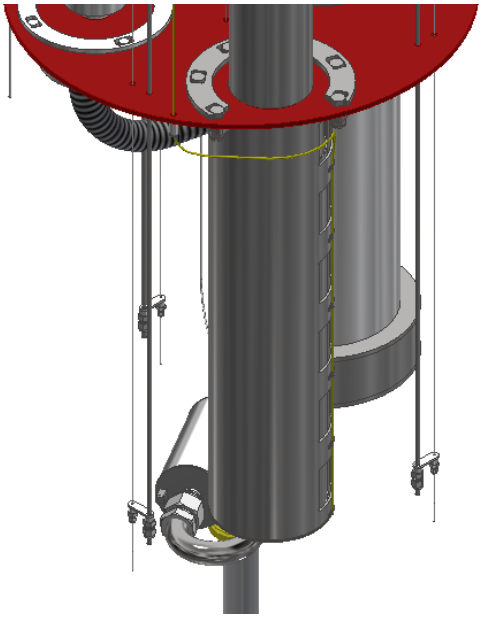

Figure 14: View of 3 optical fiber capillaries coupled to 1/4" multipoint thermocouple probes

A custom sprung bellows assembly has been designed to provide tension and to make up any thermal expansion differential between the 1/16" capillary tubes in ports 3, 7, 10, 13, and 14 and the rest of the primary vessel components, Figure 15 and Figure 16. The total capillary length is approximately 2 meters. Assuming an extremely conservative temperature differential between capillary and inner vessel side walls of 250 °C, the maximum thermal expansion differential can be calculated as 0.32" using a thermal expansion coefficient for stainless steel of 1.6 E-5 m/m-K. Thus the bellows and spring should be able to account for expansion and contraction over a range of 0.32" x 2 = 0.64". A high temperature Inconel 600 spring with a free length of 1.75", maximum

deflection of 0.93” and linear spring rate of 12 lbs/in was sourced. To ensure the spring would not permanently damage the capillary under tension a creep stress of 160 MPa was used (1% creep rate in 10,000 hours at 550 C) to determine maximum spring force allowable on the 1/16” OD, 0.009” wall capillary. The maximum permissible deflection for the spring to prevent creep damage to the capillary tube at high temperature was calculated as 2.93” using Eq 3. This is greater than the maximum spring deflection of 0.93”, thus it would not be possible to yield the capillary tubes with this assembly, even at elevated temperatures.

$$\delta_{max} = \frac{\sigma_{creep} A_{capillary}}{\gamma} \tag{3}$$

Where σ_{creep} is the stress at 1% creep rate, $A_{capillary}$ is the cross sectional area of the capillary tube, and γ is the linear spring coefficient.

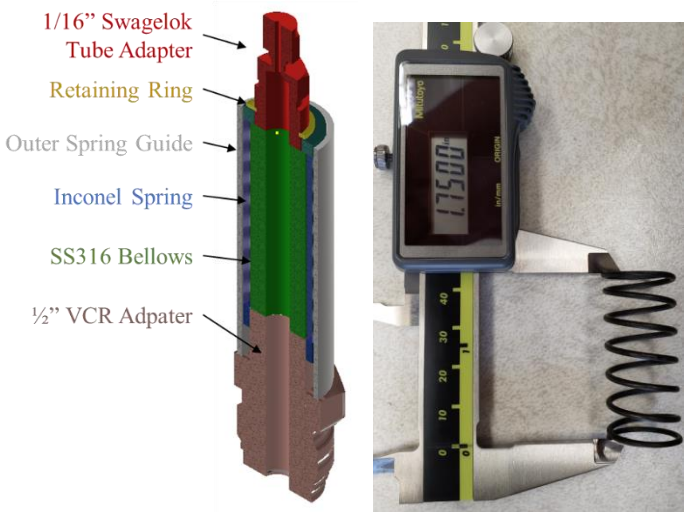

Figure 15: Sprung bellows to makeup thermal expansion differential of 1/16" capillaries, left. High temperature Inconel spring photo, right.

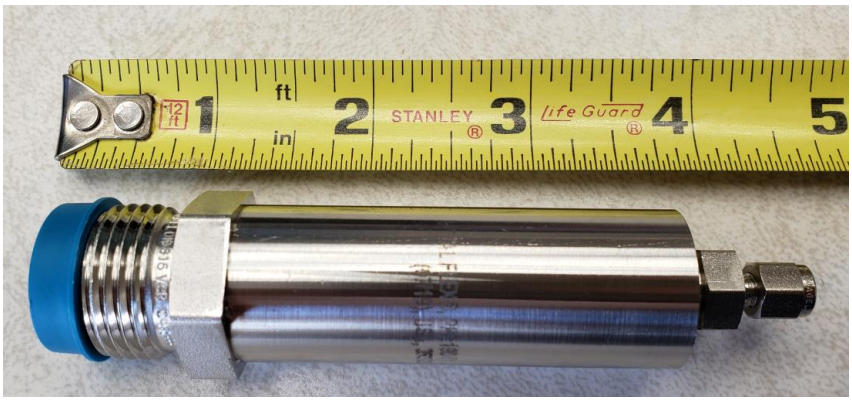

Figure 16: Picture of sprung bellows adapter

3.2. Intermediate Heat Exchanger

An intermediate heat exchanger has been designed to transfer heat from the THETA primary sodium to its secondary sodium system. As can be seen in Figure 17, the current design is a shell and tube type, with primary sodium on the shell side, and secondary sodium through a single U-tube. Baffles with a 1/2 shell window cross section are used to promote thermal mixing in the primary sodium, the top baffle possessing a deflector to prevent hot sodium impingement on the cold secondary sodium downcomer tube, Figure 18. Thermal mixing of low Prandtl number fluids can create a phenomenon known as thermal striping, where large magnitude temperature oscillations occur. With high convection heat transfer inherent to liquid metals, a significant amount of thermal stress can occur in piping [3]; the thermal striping deflector on the top baffle prevents hot sodium entering the shell side from impinging directly on the cold secondary sodium downcomer, thus reducing the thermal striping behavior. An expansion bellows on the secondary sodium upcoming tube allows for the large thermal expansion differential between the two sides of the U-tube. The design facilitates a 1/2" rod running concentric down the length of the shell to allow for adjustment of the IHX primary sodium outlet elevation into the cold pool, as will be discussed in a later section.

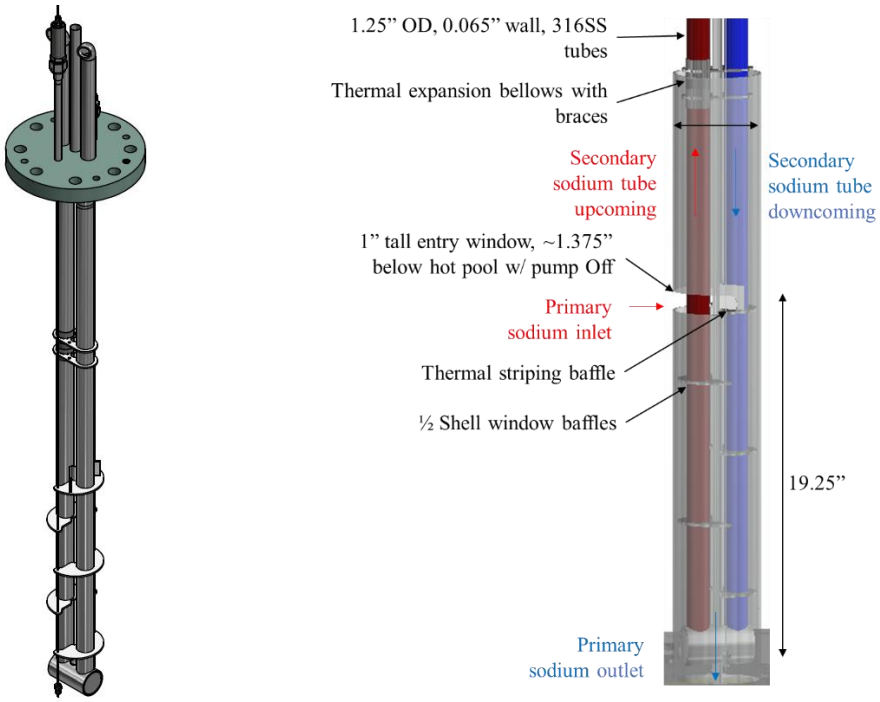

Figure 17: Shell and tube intermediate heat exchanger

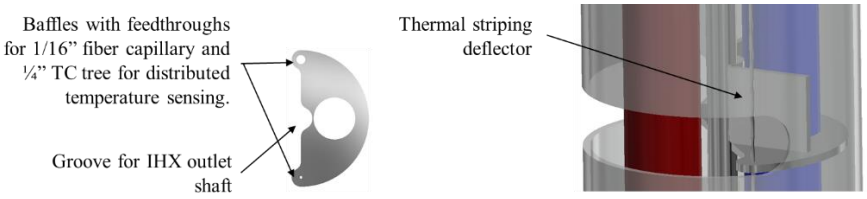

Figure 18: Intermediate heat exchanger shell side baffle, left. Top baffle showing thermal striping deflector feature, right.

The heat exchanger was sized using the effectiveness-NTU method for one shell pass and two tube passes (single U-tube). This method identifies the maximum possible heat transfer rate and uses a calculated effectiveness to determine the actual heat transfer rate, Eq. 4.

$$\dot{q} = \varepsilon \dot{q}_{max} \tag{4}$$

The effectiveness for a heat exchanger of this type as a function of transfer units and capacity ratio can be found in Eq. 5.

$$\varepsilon = 2\left[1 + C_R + \sqrt{1 + {C_R}^2}\,\frac{1 + \exp\left(-NTU\sqrt{1 + {C_R}^2}\right)}{1 - \exp\left(-NTU\sqrt{1 + {C_R}^2}\right)}\right]^{-1} \tag{5}$$

Where C_R is a dimensionless number referred to as the capacity ratio, comparing the capacitance rates of the tube and the shell side fluids, Eq. 6, and NTU is the number of transfer units, calculated using Eq. 7.

$$C_R = \frac{\dot{C}_{min}}{\dot{C}_{max}} \tag{6}$$

Where $\dot{C}_{min}$ and $\dot{C}_{max}$ are the minimum and maximum of the capacitance rates of fluid on either side of the heat exchanger.

$$NTU = \frac{UA}{\dot{C}_{min}} \tag{7}$$

The conductance of the heat exchanger, UA, is a function of both geometry and heat transfer in the heat exchanger. The conductance may be found by taking the inverse of the total thermal resistance, Eq. 8.

$$UA = \frac{1}{R_{tot}} = \frac{1}{R_{h,tube} + R_k + R_{h,shell} + R_f} \tag{8}$$

Where $R_{h,tube}$ is the convection resistance from the tube fluid to the tube inner wall, R_k is the resistance to conduction in the tube wall, $R_{h,shell}$ is the convection resistance from the shell fluid to the tube outer wall, and R_f is the resistance due to fouling. According to literature the fouling resistance in alkali metal heat exchangers is negligible if oxide level is kept below a few wppm

[8]. The convection resistance may be determined with the use of the Nusselt number. On the tube side, the Nusselt number was found using a correlation for NaK flowing through a tube [9], Eq. 9.

$$Nu = 4.82 + 0.0185 \cdot Pe^{0.827} \quad (9)$$

On the shell side, the Nusselt number was found using a correlation for in-line flow through un-baffled rod bundles in wide spaced arrays (tube pitch / tube diameter = P/D > 1.35) [10], Eq. 10. Note that P/D for the above THETA IHX is 1.6.

$$Nu = 6.66 + 3.126\frac{P}{D} + 1.84\left(\frac{P}{D}\right)^2 + 0.0155(\bar{\varphi}Pe)^{0.86} \quad (10)$$

Where $\bar{\varphi}$, the ratio between eddy diffusivities of heat and momentum, is generally assumed equal to one [11].

Kern's method was used to estimate shell side pressure drop across the heat exchanger, Eq. 11 [12].

$$\Delta P_{Kerns} = 8 j_f \left(\frac{D_s}{d_e}\right)\left(\frac{L}{l_B}\right)\frac{\rho {u_s}^s}{2}\left(\frac{\mu}{\mu_w}\right)^{-0.14} \quad (11)$$

Where j_f is a friction factor found using Figure 19 [12], D_s is the shell side inner diameter, d_e is the hydraulic diameter, L is the tube length, l_B is the baffle spacing, ρ is the process fluid density, u_s is the shell side linear velocity, and $\frac{\mu}{\mu_w}$ is a ratio of viscosity in the bulk fluid as compared to viscosity at the wall—in general this term may be neglected for low viscosity fluids such as sodium.

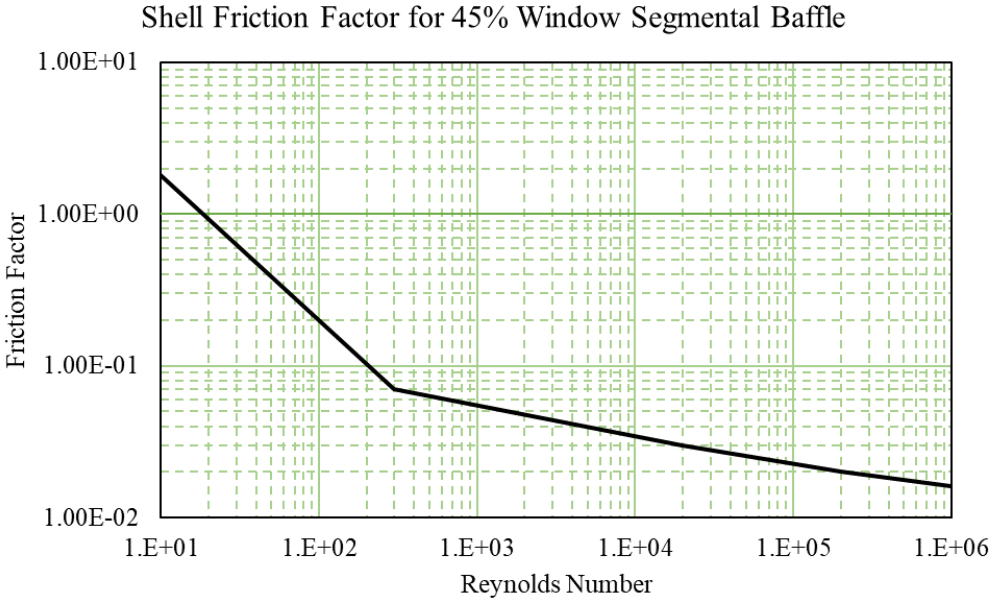

Figure 19: Shell side friction factors, segmental baffles, adapted from [12]

Alternatively, and as a second check, the pressure drop across the shell side of the IHX may be approximated with the use of minor loss coefficients by treating each baffle as an expansion and contraction as the fluid flows from one baffle window to the next, Eq. 12.

$$\Delta P_{minor-loss} = N_b\left(K_{contraction} + K_{expansion}\right)\frac{\rho {u_s}^s}{2} \quad (12)$$

Where N_b is the number of baffles and $K_{contraction}$ and $K_{expansion}$ are the minor loss coefficients found in [13].

Using the thermal hydraulic parameters given in Table 5, the performance of the THETA IHX may be predicted. As can be seen the secondary sodium system flowrate was set to 5 GPM, the primary sodium inlet temperature was set to 350 °C, the secondary sodium inlet temperature was set to 250 °C. The shell side temperature differential and head as a function of shell side flow rate can be found plotted in Figure 20. As can be seen, the Kern's method and minor loss method agree very well, there is a lack of smoothness in the Kern's method curve due to slight inaccuracies in graphically calculating friction factors from Figure 19.

Table 5: Intermediate heat exchanger sizing parameters

Parameter	Value	Unit
$Q_{sodium,secondary}$	5	GPM
$T_{sodium,primary,in}$	350	°C
$T_{sodium,secondary,in}$	250	°C

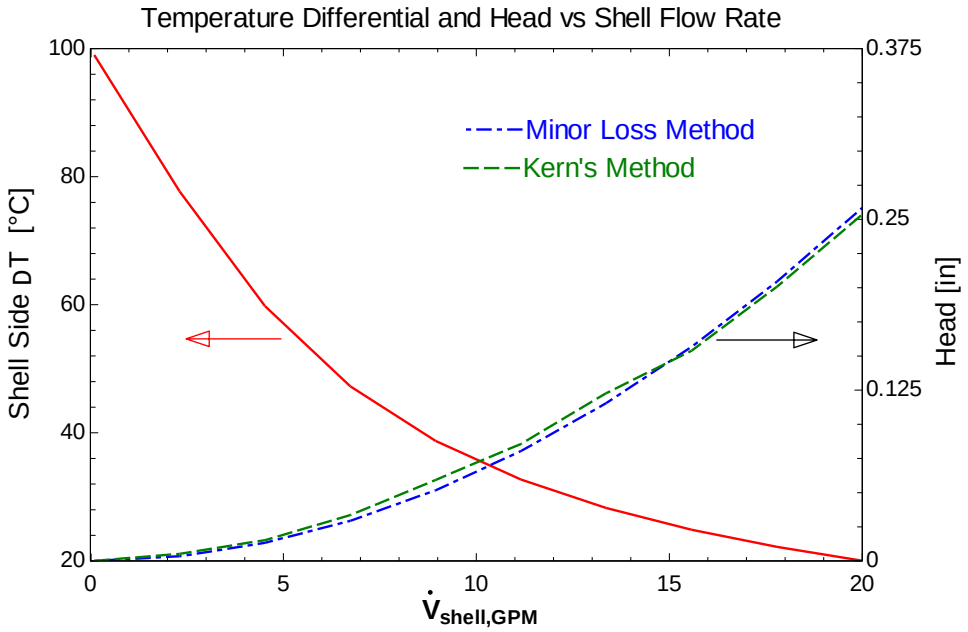

Figure 20: IHX predicted shell side temperature differential and head as a function of shell side flow rate

The IHX possesses a variable height outlet mechanism allowing for deposition of cold sodium at various elevations in the cold pool to study the transient and steady state temperature profile which develop throughout an SFR as a result of changing this variable, Figure 21. Depositing cold sodium at a lower elevation in the cold pool is predicted to result in more stratification and ultimately result in a more thermally stratified hot pool. This will be an important variable to study for the development of reactor codes. Figure 22 shows drawings of the inner and outer barrel. As can be seen there are qty. (6) 2.75" square windows at elevations spaced 4.5" apart from center to center. The inner barrel rests on a stainless steel cone on the bottom of the outer barrel in a Hastelloy C-276 seat, reducing the likelihood of galling.

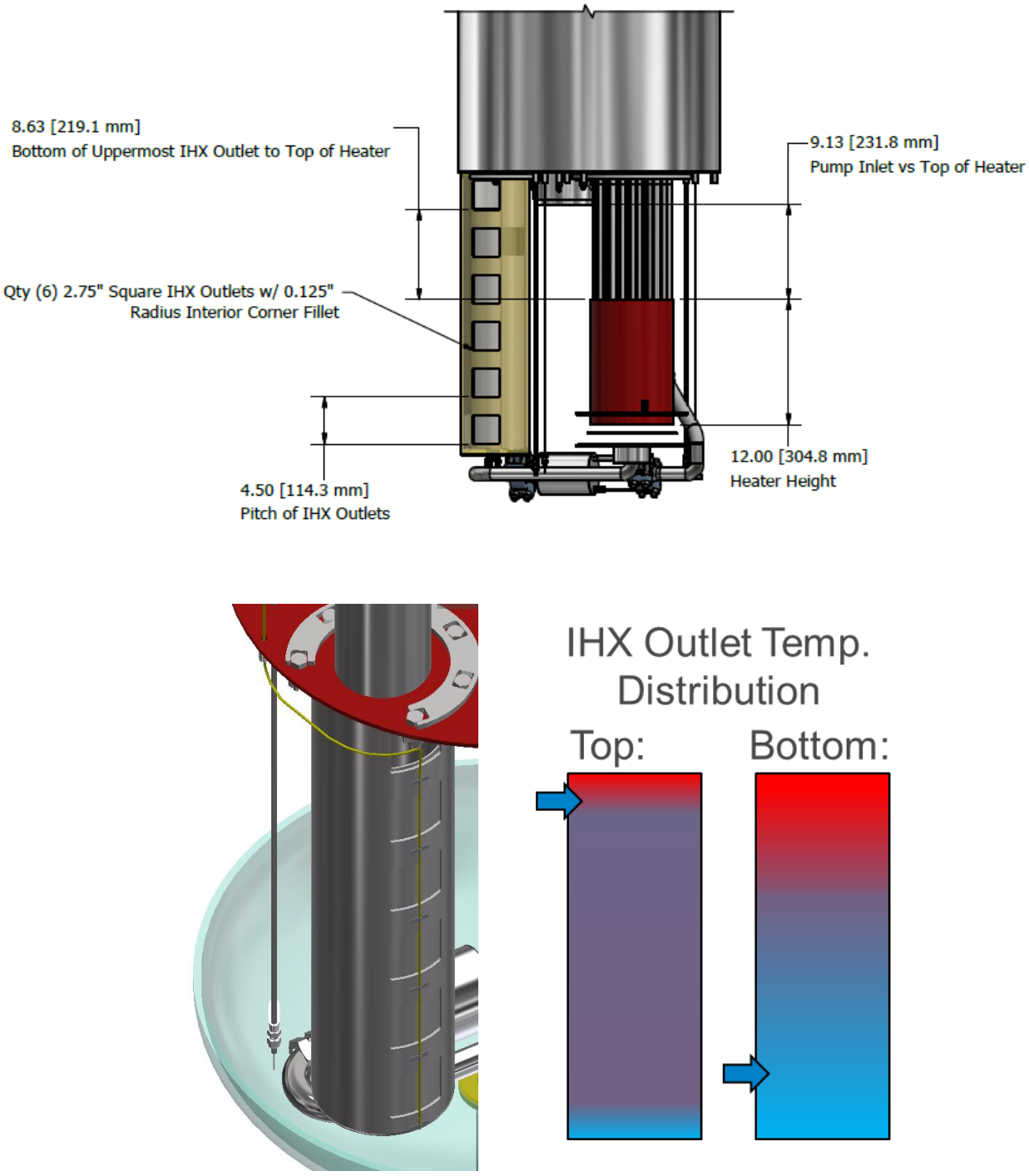

Figure 21: IHX Outlet dimension, top. Isometric model of variable elevation IHX outlet, bottom left. Drawing showing predicted cold pool temperature distribution as a function of IHX outlet window elevation, (red = hot, purple = warm, blue = cold), bottom right.

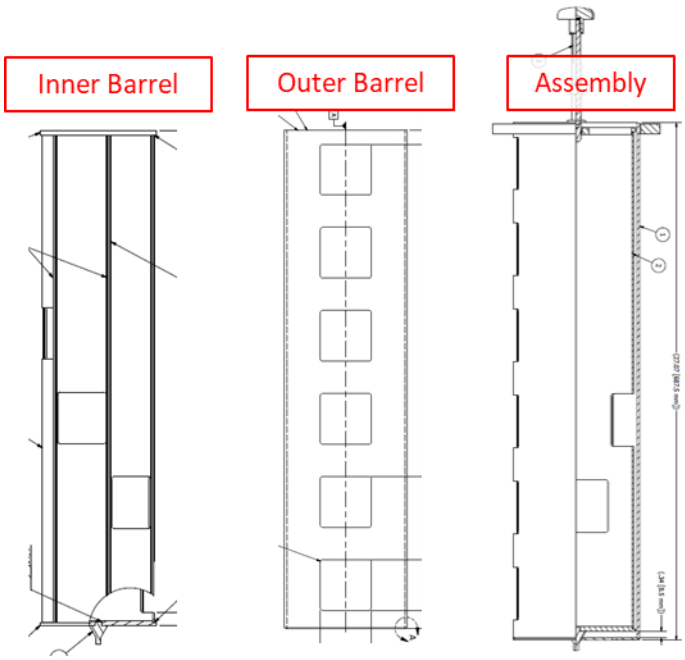

Figure 22: Variable elevation IHX outlet. Drawings showing the inner barrel, left, outer barrel, middle, and the assembly of inner/outer barrel and actuator stem, right.

3.3. CFD Analysis of Hot Pool

A computational fluid dynamic simulation was performed with Ansys CFX 19.2 to assess the performance of the intermediate heat exchanger and acquire a preliminary predicted temperature distribution of the hot pool during steady state operation of THETA. The domains, boundary conditions and meshing from this analysis are shown in Figure 23. As can be seen an adiabatic 'flow-blocker' simulating the heater element spacer plate, and ultimately the UIS of an SFR, was added to distribute flow more realistically in the hot pool. The mesh was constructed of 815,325 tetrahedral elements utilizing inflation layers in and around the IHX to accurately capture the low Prandtl number heat transfer in this region. All sodium thermal hydraulic material properties were set to a constant value for sodium at 300 °C, these values taken from [6].

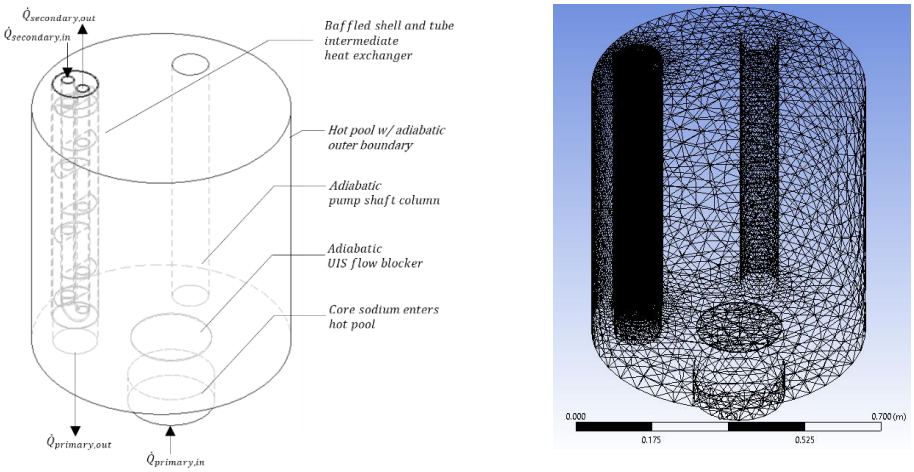

Figure 23: THETA CFD domains and boundary conditions (left), mesh wireframe showing high mesh density near IHX (right)

The CFD simulation flowrate and temperature inputs for the primary and secondary sodium domains have been provided in Table 6. These parameters were also used for analytical calculations using heat exchanger correlations as previously detailed in Section 3.2 of this report.

Table 6: CFD and analytical calculation input parameters

CFD and Analytical Inputs:		
Primary Flow Rate	5	GPM
Secondary Flow Rate	5	GPM
Primary Inlet Temp	270	°C
Secondary Inlet Temp	200	°C

Temperature and velocity profiles of interest have been highlighted in Figure 24. As can be seen, a stratified temperature profile develops in the bulk sodium of the hot pool. Downward velocity streamlines are visible in close proximity to the IHX, showing a developed large scale natural convection driven flow.

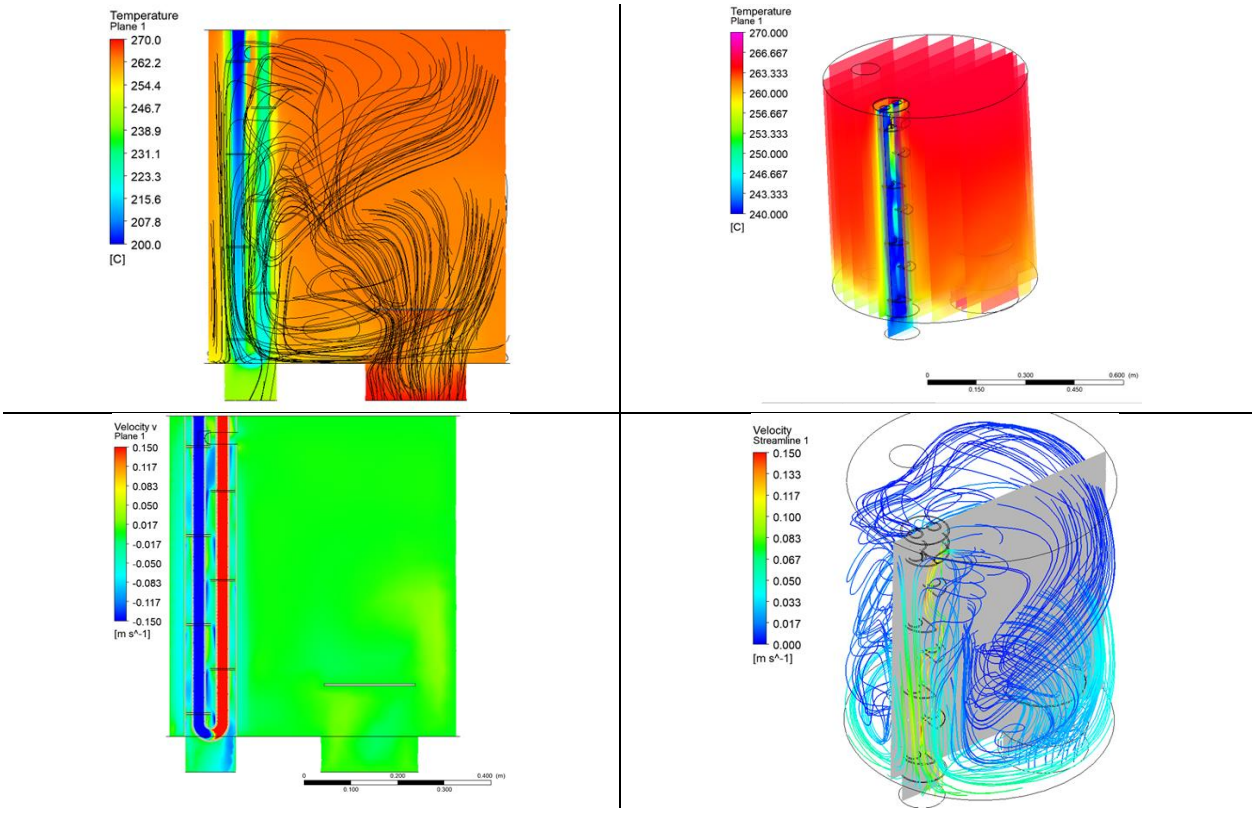

Figure 24: Temperature profile of hot pool and IHX with velocity streamlines (top,left), 3D temperature profile (top,right), velocity profile of hot pool and IHX (bottom, left), velocity streamlines of hot pool and IHX (bottom, right)

A summary of the average primary sodium outlet temperature from the IHX found with CFD and by analytical heat exchanger correlations, method detailed in the Section 3.2, can be found in Table 7. As can be seen the two analysis methods show great correlation, with the average outlet temperature within 2 °C.

Table 7: CFD and analytical results showing good correlation between two calculation methods

ANSYS CFX CFD Results:		
Primary Average Outlet Temp	244	°C
Primary Power Dissipation	9.5	kW
Analytical Results Using HX Correlations:		
Primary Average Outlet Temp.	242	°C
Primary Power Dissipation	10.46	kW

3.4. Submersible Flowmeter

A submersible permanent magnet flowmeter has been designed to acquire primary sodium flowrate, Figure 25. The flowmeter uses a magnetic field generated by high temperature Samarium-Cobalt (SmCo) magnets, oriented perpendicular to sodium flow, to generate a Lorentz current that is linearly proportional to flow. The measured voltage signal, V_m, is read with two pickup wires oriented diametrically across the flow tube and is related to sodium flowrate via Eq. 13 [14], [15].

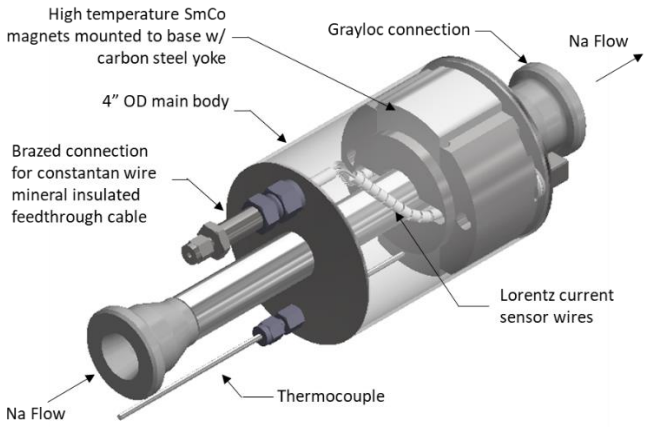

Figure 25: Submersible permanent magnet flowmeter

$$V_m = K_1 K_2 K_3 \frac{4BQ}{\pi d^2} \tag{13}$$

Where the *K* factors account for geometric and material properties, *B* is the magnetic field strength measured at the central plane of the magnets, at the center of the sodium flow, *Q* is the sodium volumetric flowrate, and *d* is the inner diameter of the sodium flow-tube. The *K* factors are given in Eqs. 13-15.

K_1, Eq. 14, accounts for the "shunting" effect, whereby the sodium containment can reduce the measured signal depending on material electrical resistivity and the geometry.

$$K_1 = \frac{2d/D}{\left[1 + \left(\frac{d}{D}\right)^2\right] + \left(\frac{\rho_f}{\rho_w}\right)\left[1 - \left(\frac{d}{D}\right)^2\right]} \tag{14}$$

Where *D* is the outer diameter of the sodium flow-tube, ρ_f is the resistivity of the liquid metal, and ρ_w is the resistivity of the containment material. As the permanent magnets are not infinitely long, end effects are accounted for with K_2, Eq. 15.

$$K_2 = -0.0047\left(\frac{L}{d}\right)^4 + 0.0647\left(\frac{L}{d}\right)^3 - 0.3342\left(\frac{L}{d}\right)^2 + 0.77 \tag{15}$$

Where L is the length of the permanent magnets in the direction of sodium flow. K_3, Eq. 16, accounts for temperature effect on the permanent magnet.

$$K_3 = \frac{(-7E-07)T^3 - 0.0002T + 0.8587}{0.8587} \tag{16}$$

Where T is the temperature of the permanent magnet in degrees Celsius. Eq. 16 was found by fitting a quadratic function to the residual induction as a function of temperature, as provided by the manufacturer, Figure 26. The particular magnetic material used in this flowmeter is from Electron Energy Corporation, product number EEC SmCo 2:17-18 T550. This grade of SmCo has shown resistance to magnetic field degradation with a neutron flux of 10^{18} n/cm^2 and temperatures ≤ 550 °C [16].

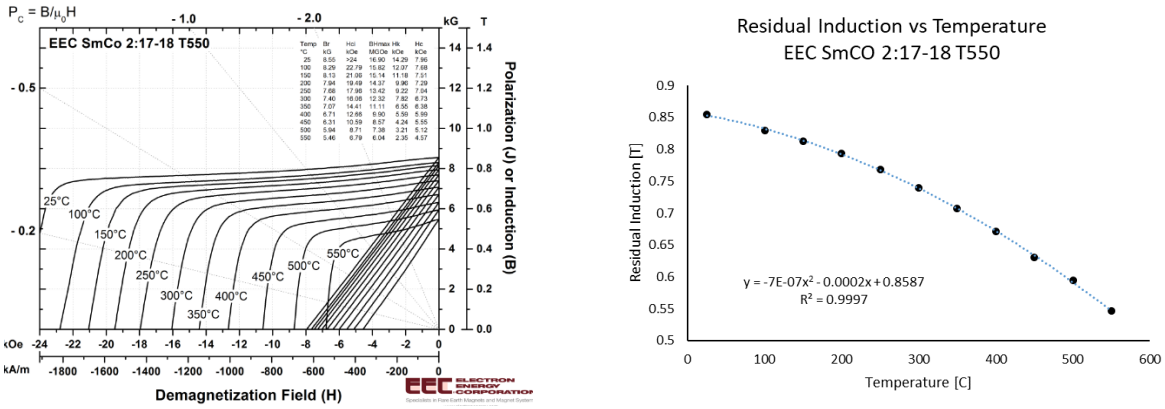

Figure 26: Manufacturer (Electron Energy Corporation) provided BH curve as a function of temperature, left. Residual induction as a function of temperature for SmCo T550 high temperature magnets from Electron Energy Corporation, right.

In order to acquire the magnetic field at the flowmeter center, an Ansys Maxwell finite element simulation was performed to calculate 3D magnetic flux field, Figure 27. The flux density at the center of the flow tube along the center plane of the magnets was calculated as 0.288 T. Using an F.W. Bell 5180 Gaussmeter, the magnetic flux at the center position of the as built magnet assembly was measured as 0.259 T, Figure 28.

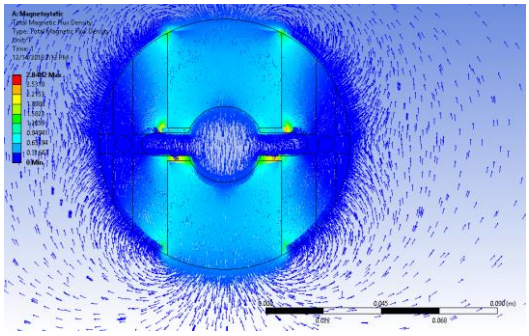

Figure 27: Finite element analysis of permanent magnets installed in carbon steel yoke in air. Mesh size of 2mm used. Magnetic flux calculated at central position: 0.288 T.

Figure 28: Measuring magnetic field of magnets in yoke with F.W. Bell 5180 Gaussmeter

Using Eqs. 12-15 and a value of 0.259 T for the magnetic field, the flowmeter induced voltage as a function of flow rate and temperature may be determined, Figure 29. As seen in literature, there can be discrepancies in the predicted vs. actual voltage as a function of flowrate curves, therefore the flowmeter will be calibrated against a NIST traceable vortex shedder flowmeter in sodium [3]. However, the predicted voltage signal is quite strong with a voltage of 75-150 mV predicted at 5 GPM (depending on temperature).

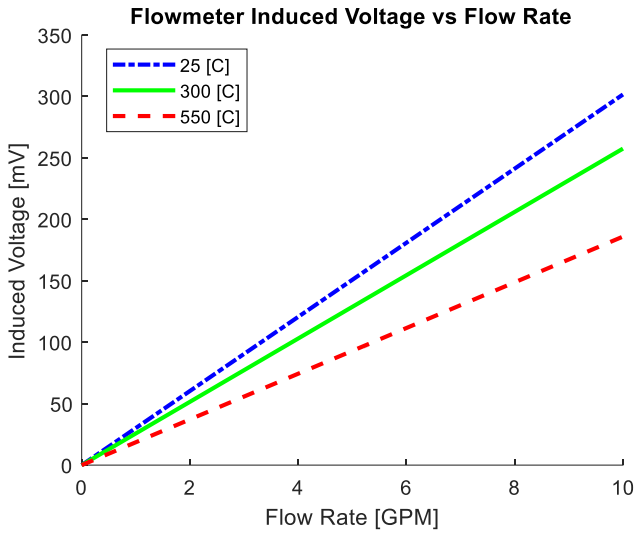

Figure 29: Voltage signal as a function of sodium flow rate and temperature

Samarium cobalt magnets possess a strong pull force, thus precautions must be taken when assembling the flowmeter yoke to prevent injury and/or damage to the brittle magnets. As can be seen in Figure 30, a wooden jig for assembling the magnet assembly was constructed; wooden tracks were used to direct the magnet into position on the yoke, using plastic shims to slowly allow the magnet to approach the yoke. The yoke/magnet assembly may then be slid into the outer tube for final seal welding with top cap, Figure 31.

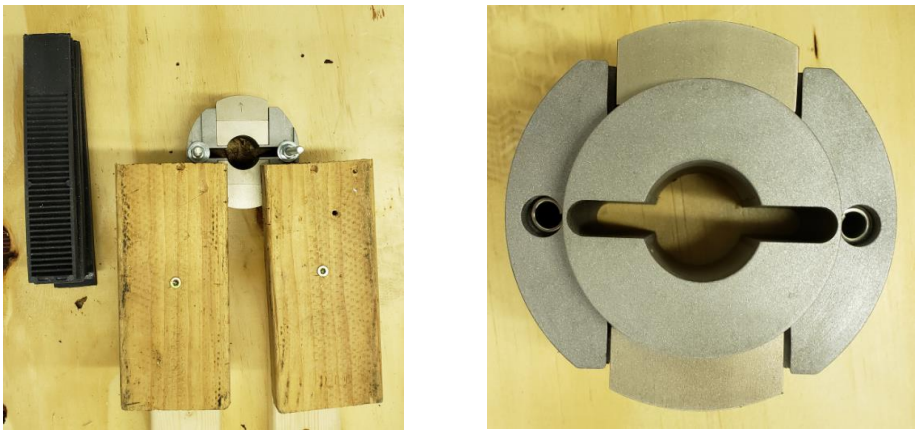

Figure 30: Magnet/yoke assembly using wooden tracks and plastic shims, left. Assembled magnet/yoke assembly, right.

Figure 31: Magnet/yoke installation, left. Top cap prepared for final welding, right.

Careful attention was paid to the method of attaching the sensor wires to the flow tube as the electrical resistance created by a poorly attached wire can affect signal readings. A series of mockups were created with various attachment techniques, Figure 32. The final attachment scheme was to weld a 0.187" diameter 'wire nub connector' with a weep hole, then braze the 1/16" 316SS sensor wire to this nub connector using a high temperature (760 °C liquidous) Ag-Cu alloy, Figure 33.

Figure 32: Mockups of sensor wire attachment methods

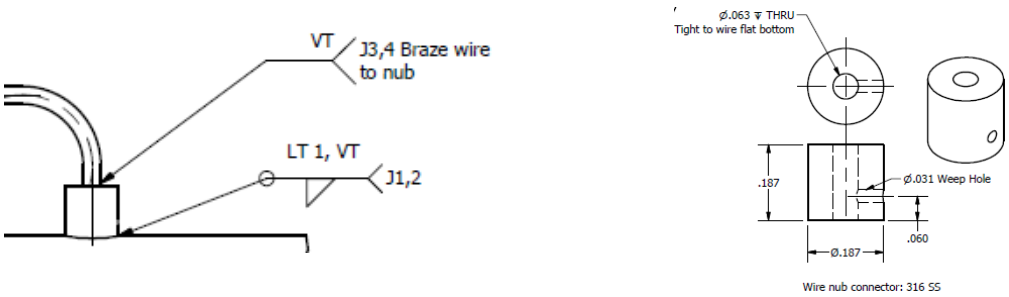

Figure 33: Connection of sensor wire to flow tube in submersible permanent magnet flowmeter. Attachment of wire nub connector via welding and brazing, left, detail drawing of wire nub connector, right.

The method for attaching the mineral insulated cable to the flowmeter feedthrough under sodium can be found in Figure 34. As can be seen a protective housing is swaged over a high temperature brazed connection between the 316SS sensor wires and the constantan wires on the MI cable.

Precautions were taken when welding the flowmeter together to avoid exposing the magnets to high temperature. Most of the flowmeter welds were made without magnets installed and during final welds, with magnets installed, copper heat sinks and a continuous argon purge over the magnets were used to dissipate welding heat, Figure 35. The magnetic field was measured post-welding and there was no detectible degradation in magnetic field strength found, Figure 35

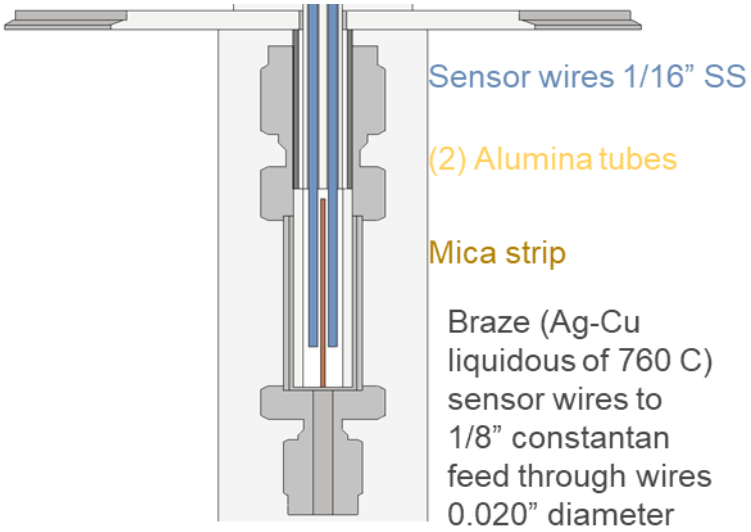

Figure 34: Sensor wire feedthrough from flowmeter to mineral insulated wire.

Figure 35: Copper heat sinks and argon purge during welding (left), magnetic field measurement post welding end cap onto outer shell

3.5. Pump

The primary sodium centrifugal pump has been received from Wenesco Inc., Figure 36, and installed in a water testing rig as seen in Figure 37. The P&ID of the flow circuit for water testing the pump can be found in Figure 37 as well which was used to develop detailed flow curves for the pump, Figure 38.

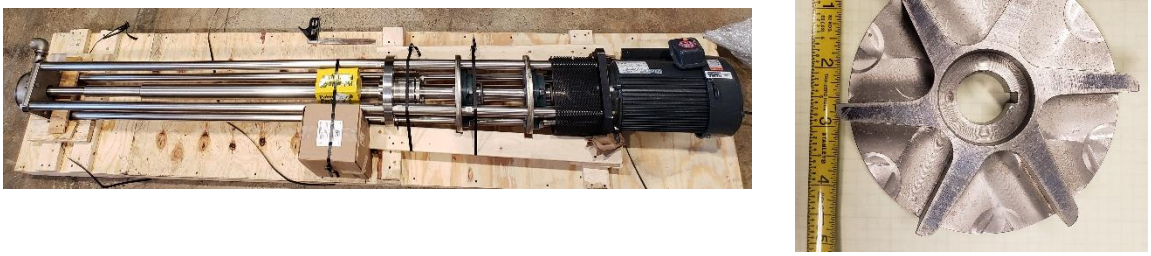

Figure 36: Pump as delivered, left, 4.5" OD impeller, right.

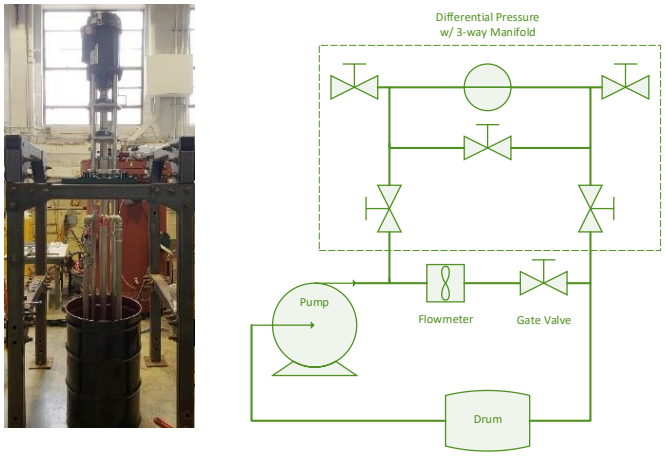

Figure 37: Wenesco centrifugal pump mounted for water testing (left). P&ID for water testing (right)

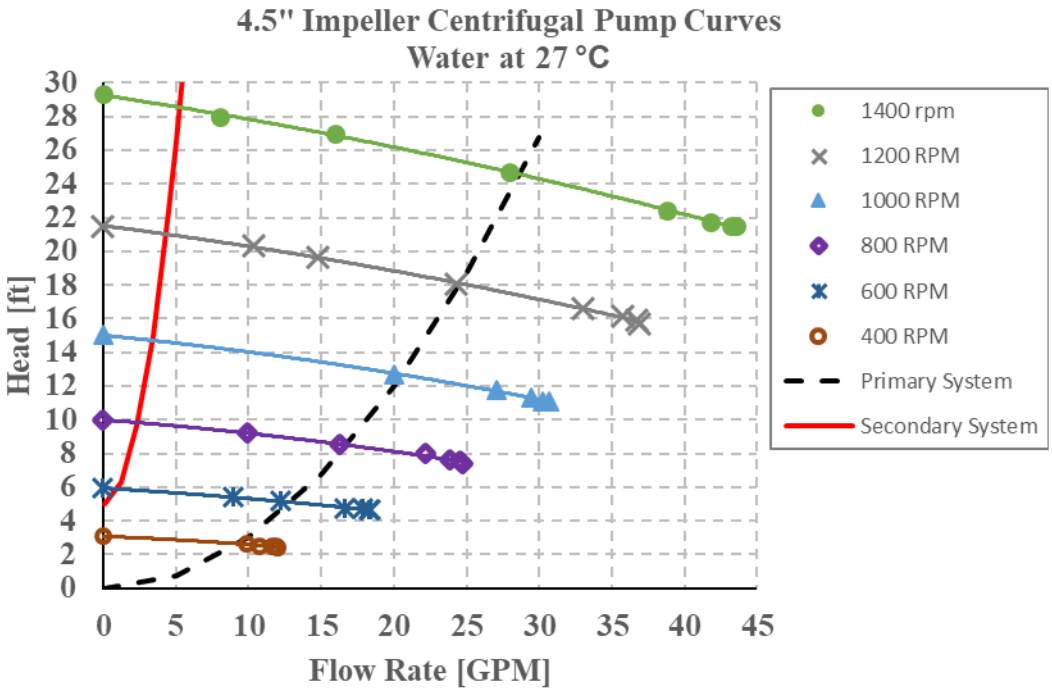

Figure 38: Pump curves made using water at 27 °C as surrogate fluid. System curves shown for primary and secondary sodium.

An all stainless steel flexible metal hose has been acquired that will be located at the pump case outlet to account for piping thermal expansion and any mechanical/hydraulic vibration, Figure 39. The electrical enclosures for THETA pump and heater control as well as data acquisition have

been completed and are currently being tested for proper functionality by performing the primary pump water testing / pump curve formulation, Figure 40.

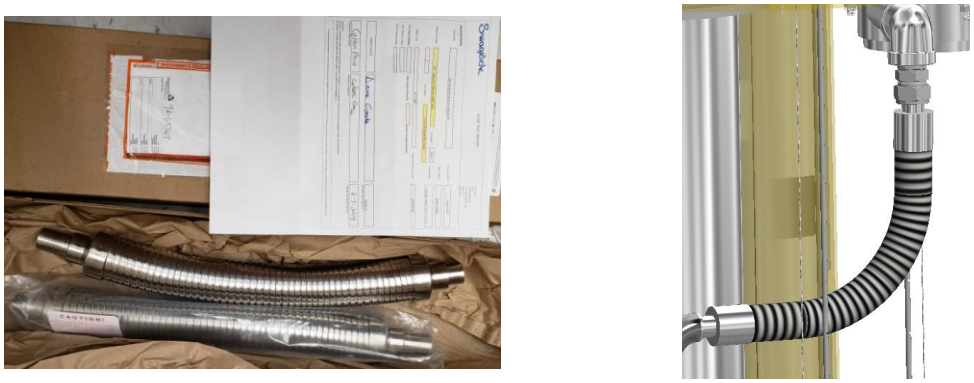

Figure 39: Swagelok FX stainless steel flexible hose for case outlet, left, model showing placement at outlet of pump case, right

Figure 40: 240 VAC, 480 VAC and 24 VDC electrical enclosures

3.6. Immersion Heater

The immersion heater and associated electrical enclosure have been received from Chromalox, Figure 41. Heater elements were tested with multimeter to ensure proper rated resistance of ~35 ohms, ensuring no significant damage resulted during shipment. The immersion heater is currently in storage in a climate controlled room with desiccant bags to prevent moisture ingress into the heater elements.

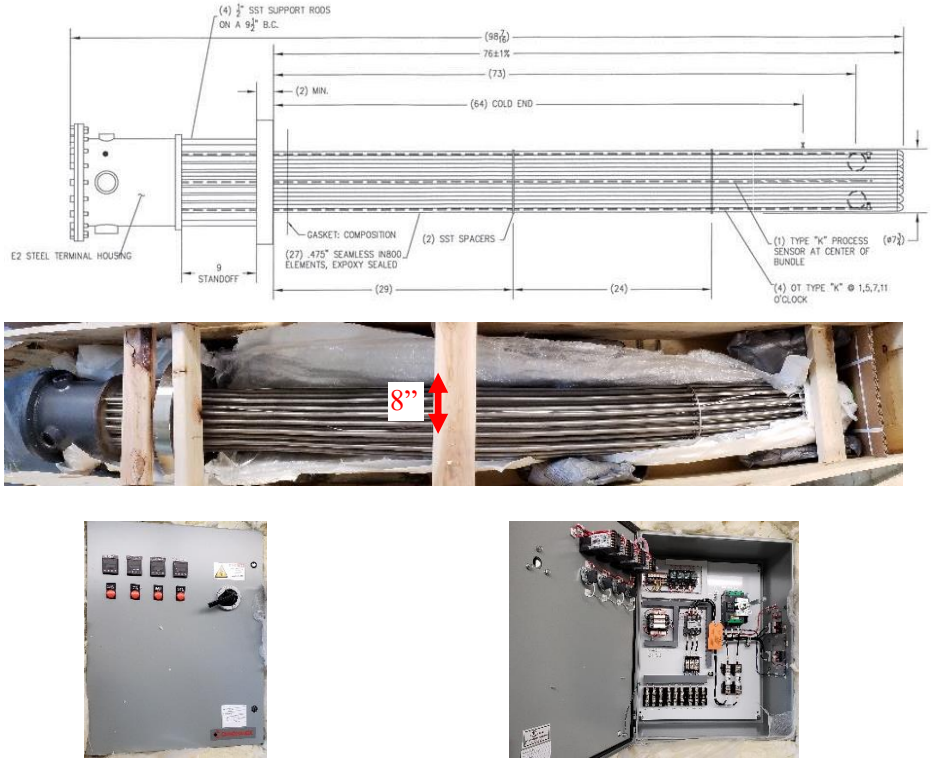

Figure 41: Chromalox 38 kW Immersion Heater (top). Heater control system electrical enclosure (bottom).

3.7. Inner Vessel Stress Analysis

A finite element analysis was performed using Autodesk Inventor's stress analysis software on inner vessel to ensure >2x factor of safety with hot pool full of sodium without any upward buoyancy force from the cold pool supporting load. The mesh, loads/constraints and safety factor (as a function of yield strength) are all detailed in Figure 42. A summary of the material property used for this analysis can be found in Table 8. The analysis showed a factor of safety of 3.1 for yield strength of 304SS at 593 °C.

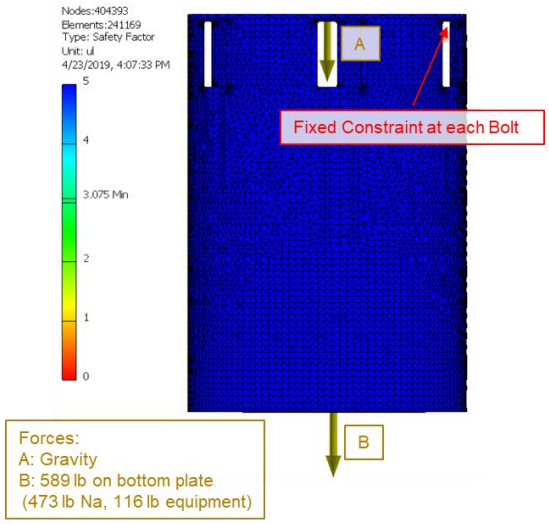

Figure 42: Inner vessel stress analysis

Table 8: Material properties for 304SS at 593 °C. Source: https://www.nickelinstitute.org/media/1699/high_temperaturecharacteristicsofstainlesssteel_9004_.pdf

Material	Yield Strength [MPa]	Density [kg/m^3]	Young's Modulus [GPa]	Poisson's Ratio [-]
304SS at 593 °C	113	7,780	158.2	0.29

4. Secondary Sodium Component Summary

4.1. Air to Sodium Heat Exchanger

A custom, U-stamped (ASME BPVC Sec. VIII Div. 2) air to sodium heat exchanger is being constructed at Enerquip LLC in Medford, Wisconsin. The heat exchanger is a tube and shell design, with sodium flowing through qty. (24), 0.75" OD x 0.049" wall, 24" long single pass seamless 316/316L SS U-tubes. The heat exchanger bonnet, tube sheet, tubes, and shell will be fully welded with RT1 radiography, hydrostatic pressure test, and helium leak check to ensure no egress of sodium during operation. The heat exchanger is rated for a maximum sodium temperature of 538 °C (1000 °F) at 100 PSIG with a maximum heat dissipation of 39 kW (133.8 kBtu/hr).

The manufacturer design drawing can be found in Figure 43. A summary of the heat exchanger sizing analysis from the manufacturer has been provided in Table 9. A summary of the maximum nozzle loads allowable on the bonnet nozzles from the sodium secondary piping has been included in Figure 44.

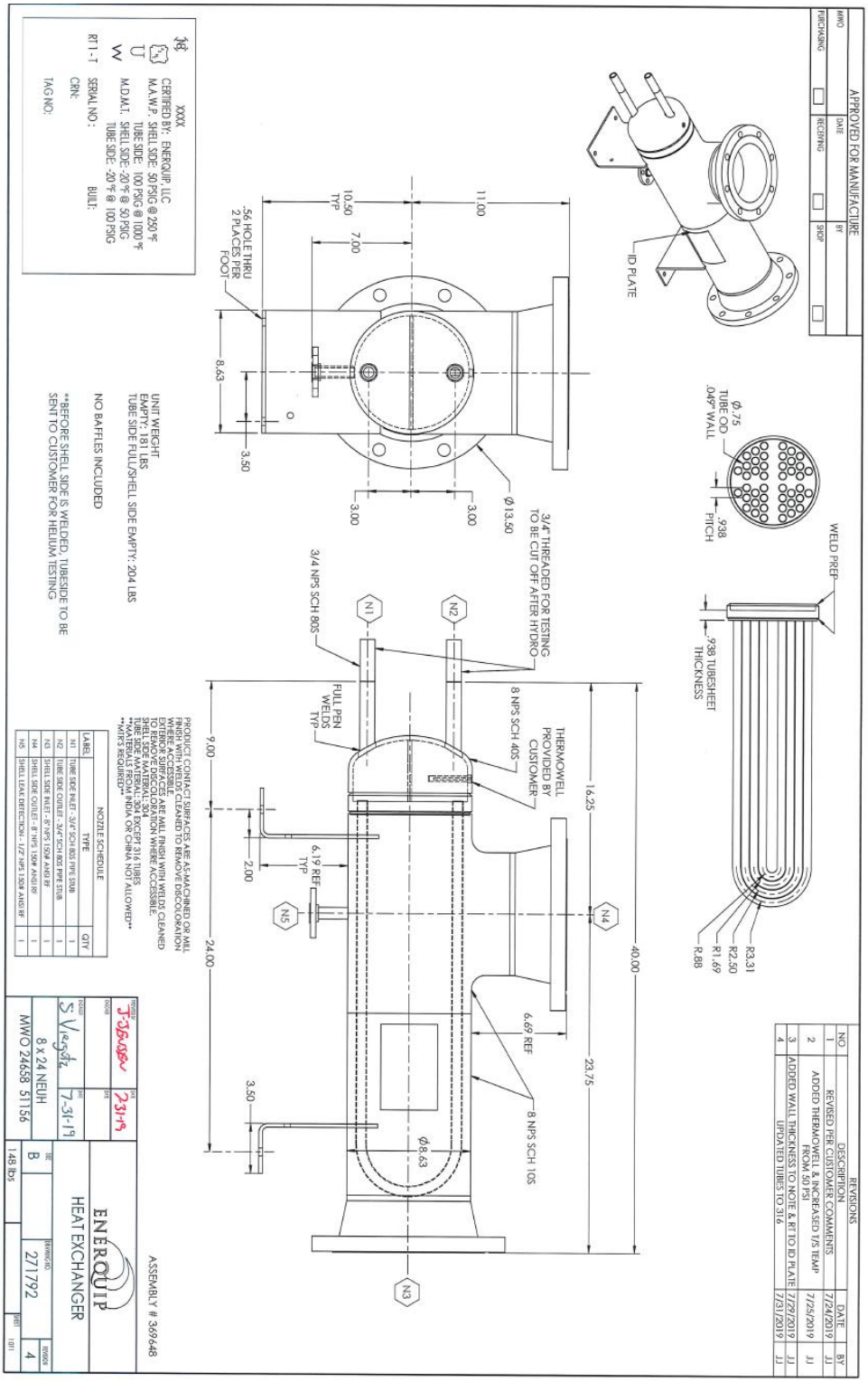

Figure 43: Manufacturer design drawing of tube-and-shell type air-to-sodium heat exchanger

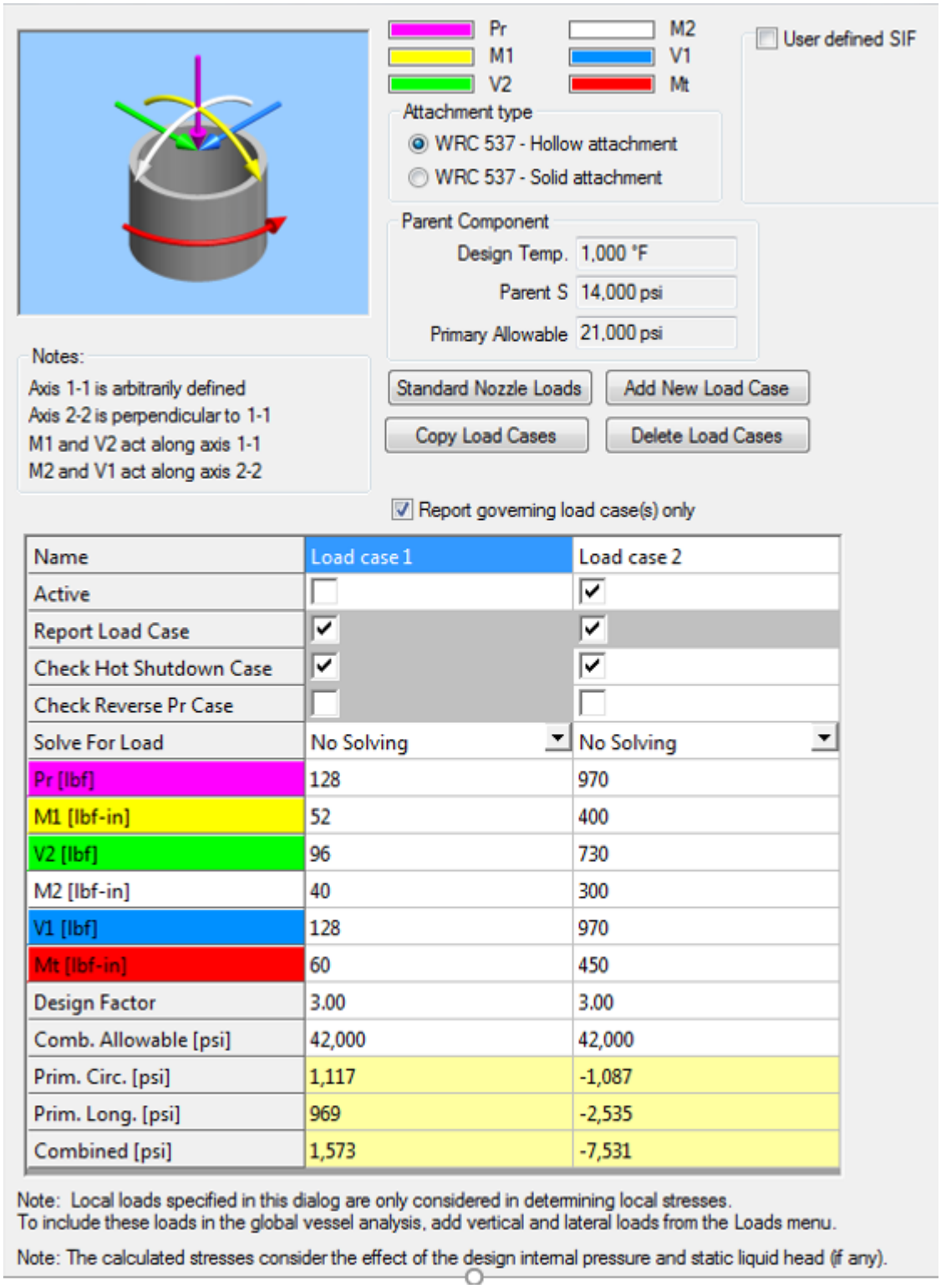

Name	Load case 1	Load case 2
Active	☐	☑
Report Load Case	☑	☑
Check Hot Shutdown Case	☑	☑
Check Reverse Pr Case	☐	☐
Solve For Load	No Solving	No Solving
Pr [lbf]	128	970
M1 [lbf-in]	52	400
V2 [lbf]	96	730
M2 [lbf-in]	40	300
V1 [lbf]	128	970
Mt [lbf-in]	60	450
Design Factor	3.00	3.00
Comb. Allowable [psi]	42,000	42,000
Prim. Circ. [psi]	1,117	-1,087
Prim. Long. [psi]	969	-2,535
Combined [psi]	1,573	-7,531

Note: Local loads specified in this dialog are only considered in determining local stresses.
To include these loads in the global vessel analysis, add vertical and lateral loads from the Loads menu.

Note: The calculated stresses consider the effect of the design internal pressure and static liquid head (if any).

Figure 44: Maximum permissible nozzle loading on AHX bonnet nozzles are given in the column for "Load case 2." This information was used to set a limit for stress imposed by secondary piping during B31.3 pipe analysis.

Table 9: Air-to-sodium heat exchanger specification sheet

HEAT EXCHANGER SPECIFICATION SHEET Page 1 **US Units**

						Job No.					
Customer	Argonne National Laboratory					Reference No.	Matt Weathered				
Address						Proposal No.	51156R2				
Plant Location	Argonne, IL 60439					Date	5/31/19		Rev		
Service of Unit	Cooler					Item No.					
Size	8.329 x 24	inch	Type	BEU	Vertical	Connected In	1	Parallel	1	Series	
Surf/Unit (Gross/Eff)	19.218 / 18.678	ft2	Shell/Unit	1		Surf/Shell (Gross/Eff)	19.218 / 18.678	ft2			

PERFORMANCE OF ONE UNIT

Fluid Allocation		Shell Side		Tube Side	
Fluid Name		1200 SCFM Air		5 gpm Liquid Sodium	
Fluid Quantity, Total	lb/hr	5400.0		2102.0	
Vapor (In/Out)		5400.0	5400.0		
Liquid				2102.0	2102.0
Steam					
Water					
Noncondensables					
Temperature (In/Out)	F	77.00	180.12	1000.0	790.00
Specific Gravity				0.8262	0.8533
Viscosity	cP	0.0186	0.0212	0.2240	0.2670
Molecular Weight, Vapor					
Molecular Weight, Noncondensables					
Specific Heat	Btu/lb-F	0.2390	0.2416	0.3009	0.3055
Thermal Conductivity	Btu/hr-ft-F	0.0151	0.0176	36.044	39.482
Latent Heat	Btu/lb				
Inlet Pressure	psia	16.496		24.696	
Velocity	ft/sec	84.12		0.22	
Pressure Drop, Allow/Calc	psi	10.000	0.782	10.000	0.036
Fouling Resistance (min)	ft2-hr-F/Btu	0.00050		0.00200	

Heat Exchanged	133830	Btu/hr		MTD (Corrected)	760.1	F	
Transfer Rate, Service	9.43	Btu/ft2-hr-F	Clean	20.50	Btu/ft2-hr-F	Actual	19.39 Btu/ft2-hr-F

CONSTRUCTION OF ONE SHELL — Sketch (Bundle/Nozzle Orientation)

			Shell Side	Tube Side
Design/Test Pressure		psig	50.000 /	50.000 /
Design Temperature		F	250.00	1000.0
No Passes per Shell			1	2
Corrosion Allowance		inch	0.0000	0.0000
Connections	In	inch	1 @ 8.0000	1 @ 1.0000
Size &	Out	inch	1 @ 8.0000	1 @ 1.0000
Rating	Intermediate		@	@

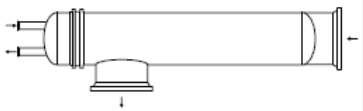

Tube No.	22U	OD	0.7500	inch	Thk(Avg)	0.0490	inch	Length	2.000	ft	Pitch 0.9375 inch
Tube Type	Plain				Material	SA-213 TP304L Tube (S) S30403					Tube pattern 60
Shell	SA-312 TP304L Pipe (W) S30403	ID	8.3290	OD	8.6250	inch	Shell Cover				(Integ.)
Channel or Bonnet	SA-240 304L Pl. S30403						Channel Cover				
Tubesheet-Stationary	SA-240 304L Pl. S30403						Tubesheet-Floating				
Floating Head Cover							Impingement Plate	None			
Baffles-Cross				Type	None	%Cut (Diam)		Spacing(c/c)	25.944	Inlet	inch
Baffles-Long						Seal Type	None				
Supports-Tube						U-Bend				Type	None
Bypass Seal Arrangement	0	pairs seal strips				Tube-Tubesheet Joint	Expanded and seal welded (2 grooves)				
Expansion Joint						Type					
Rho-V2-Inlet Nozzle	222.48	lb/ft-sec2				Bundle Entrance	0.00	Bundle Exit	0.00	lb/ft-sec2	
Gaskets-Shell Side						Tube Side					
- Floating Head											
Code Requirements	ASME							TEMA Class	C		
Weight/Shell	239.92	lb		Filled with Water	337.60	lb		Bundle	67.49	lb	

Remarks (cont.) Page 2
316/316L SA-213 seamless tubes. All 304/304L for remaining Tube Side Components
All 304/304L Shell Side Components
Industrial Finish: All surfaces are as machined or mill finish with welds cleaned to remove discoloration where accessible.
All Welded tubesheet and bonnet. Non removable.
NPS 300# ANSI Flange Tube Side Connections
NPS 150# ANSI Flange Shell Inlet
NPS 150# ANSI Flange Shell Outlet
NPT 3000# Coupling Shell Vent
U-Stamped
No China or India materials preferred. Acceptable from Japan, Europe, Canada, Domestic.
Passivation included
3.164 gallons for tubeside holdup

4.2. Secondary Sodium Piping

The secondary sodium system transfers sodium from the tube side of the intermediate heat exchanger, then to the auxiliary 18" vessel, then to the air-to-sodium heat exchanger, then back to the intermediate heat exchanger. A thermal stress analysis has been performed on the secondary sodium system by JEH Consulting with CAESAR II computer software to acquire a Professional Engineer stamp ensuring compliance with ASME B31.3 pipe code. The piping analysis demonstrated passing of pipe code under all extreme and nominal operating conditions.

The secondary piping system is seamless 3/4" SCH 40 piping made with 316H stainless steel (ASTM 376 type 316H) given its superior strength at high temperature as compared to other grades of 300 series stainless. All of the fittings are 3/4" SCH 40 316/316L seamless tubes. Originally the fittings were specified as 316H, however during procurement it was found that these were not readily available from a domestic or DFARs compliant supplier. 316/316L (ASTM A182 Type F316 or ASTM A403 Type WP316) possesses the same strength rating as 316H up to and including 1000 °F and is more readily available, therefore the fittings were specified using this grade of stainless.

The maximum temperature limit of the system is 1000 °F and the system has a design pressure of 50 PSIG. A total of six scenarios were identified for analysis to bound all possible operating conditions, Table 10, Table 11. A screenshot of the CAESAR-II software setup to test Scenarios 1-6 can be found in Figure 46. Note the maximum temperature of 1000 °F and the corresponding minimum temperature of 790 °F during nominal operating conditions with the AHX operating at full duty. A screen shot of the exaggerated overall thermal expansion of the system can be found in Figure 47, and quantitative maximum expansion in the x, y, z coordinates can be found in Figure 48.

Table 10: 6 operating scenarios for secondary sodium system to test for thermal stress analysis. Locations referenced can be found in Figure 45

Scenario	Load Case	Description	Pipes and Vessel Temperatures (°F)						
			1 - IHX to 18"		2 - Bypass	3 - 18" to AHX		4 - AHX to IPX	
			PIPES	IHX Vessel	PIPES	PIPES	18" Vessel	PIPES	AHX Vessel
1	L1	Hottest	1000	1000	1000	1000	1000	1000	1000
2	L3	Both heat exchangers	1000	1000	2.1-V2 = 1000 V2-2.4 = 790	1000	1000	790	790
3	L5	Bypass IHX	1000	1000	790	1000	1000	4.1-V3 = 790 V3-4.14 = 1000	790
4	L7	Coldest	0	0	0	0	0	0	0
5	L9	Thermal Gradient I - AHX on, No pipe cooling	1000	1000	1000	1000	1000	4.1-4.3 = 790 4.3-4.14 = 1000	790
6	L11	Thermal Gradient II - IHX on, No pipe pre-heat	1.1-V1 = 1000 V1-1.6 = 790	1000	790	790	790	790	790

Table 11: Summary of operating load cases

Scenario Description	Operating Case #	CAESAR II Load Case	System Pressure	CAESAR II T Case	Constant T?
Hottest	1	L1	50 psig	T1:	YES
Both HX	2	L3	50 psig	T2:	NO
Bypass	3	L5	50 psig	T3:	NO
Coldest	4	L7	50 psig	T4:	YES
Thermal Gradiant I	5	L9	50 psig	T5:	NO
Thermal Gradiant II	6	L11	50 psig	T6	NO
Seismic	Op 1 – 6 + Seismic	L13 - L36	50 psig	T1 - T6	YES/NO

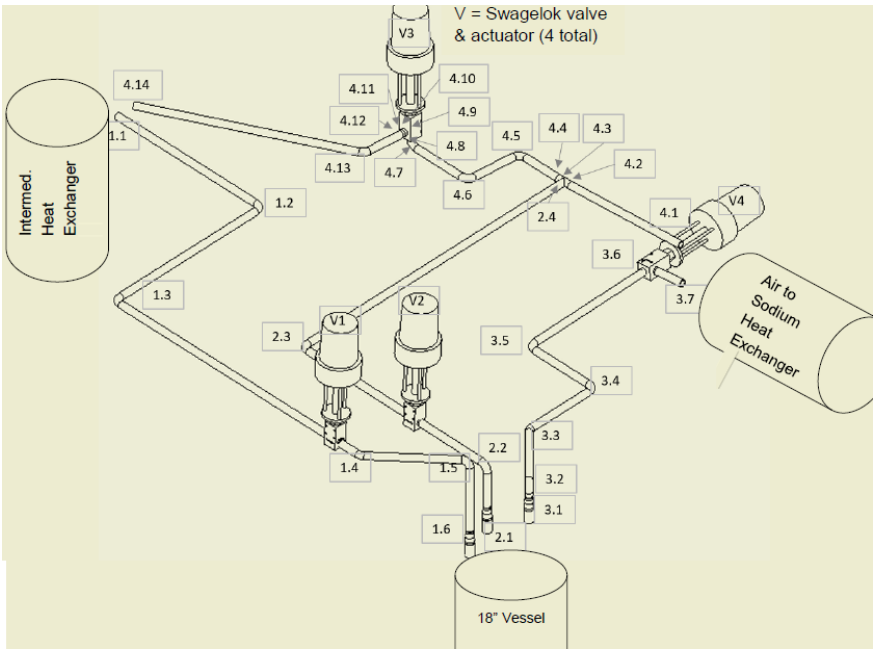

Figure 45: Piping locations for thermal stress analysis

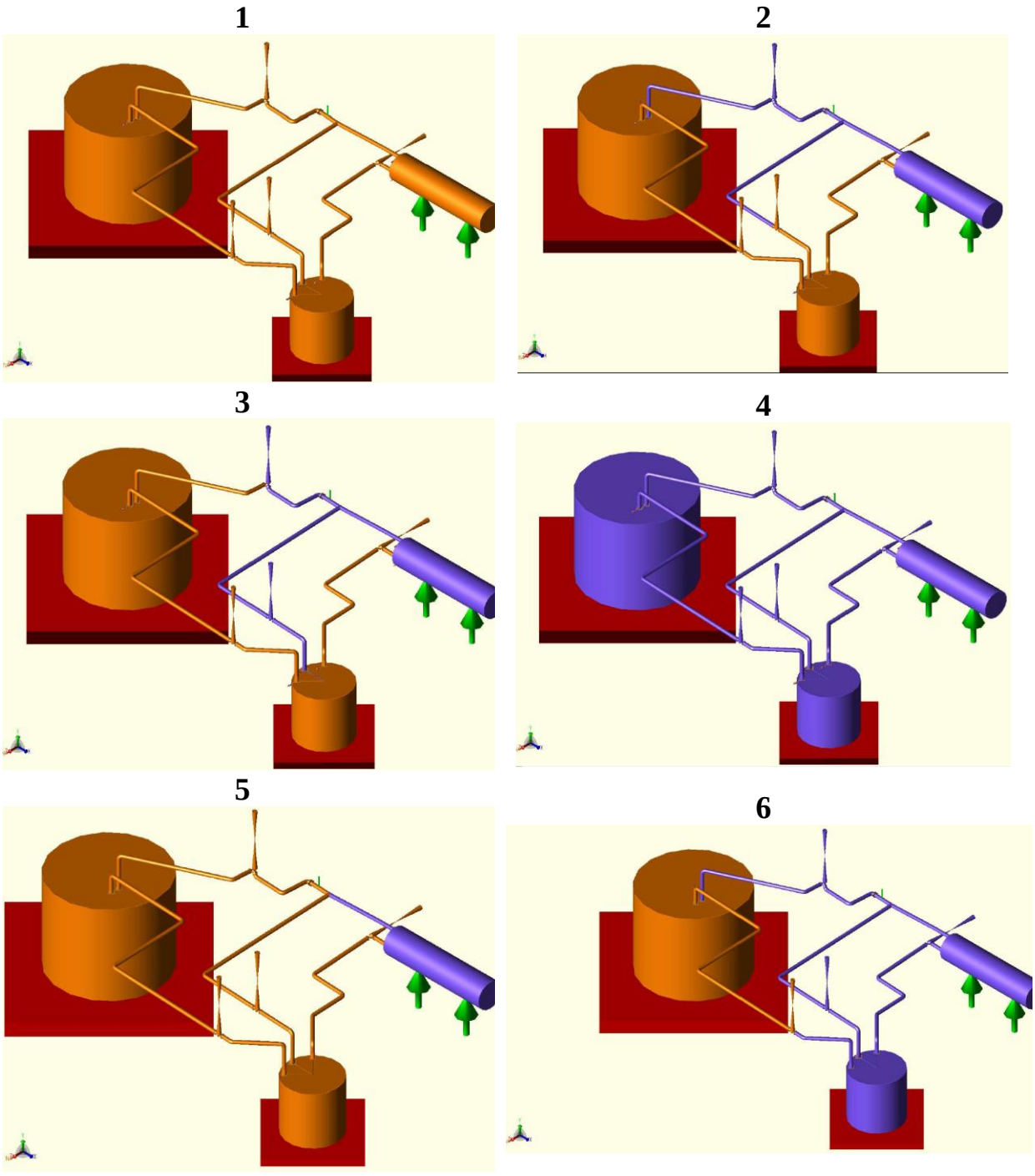

Figure 46: Screenshot of CAESAR-II software with setup for testing Scenarios 1-6. Orange = 1000 °F, purple = 790 °F, except for scenario 4 where purple = 0 °F.

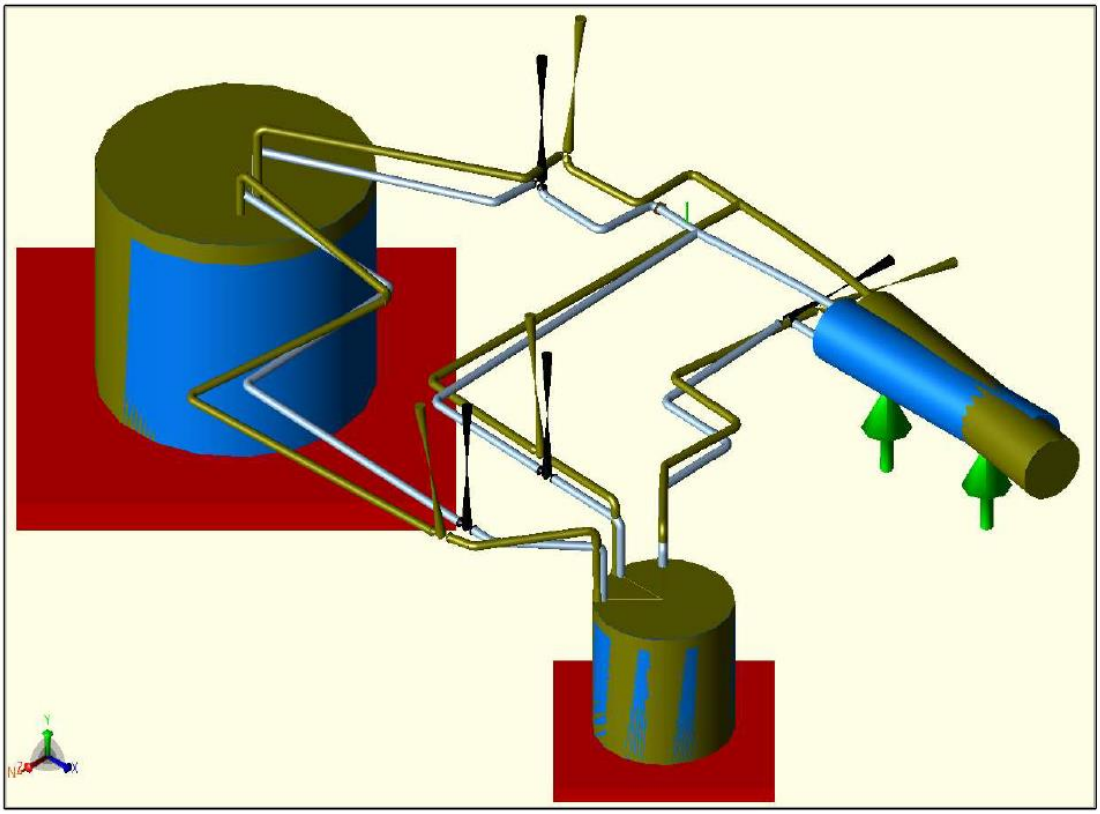

Figure 47: Visualization of thermal expansion, displacement exaggerated to allow for understanding of overall movement.

(a)

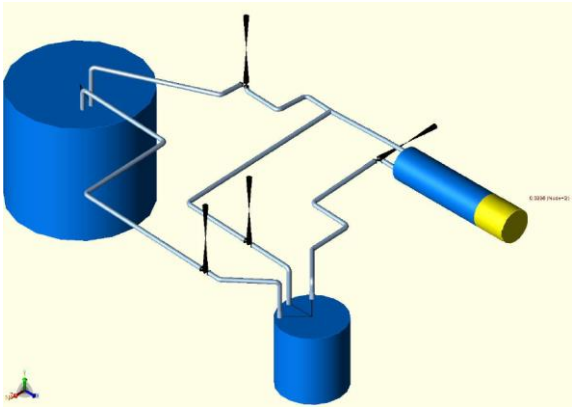

(b)

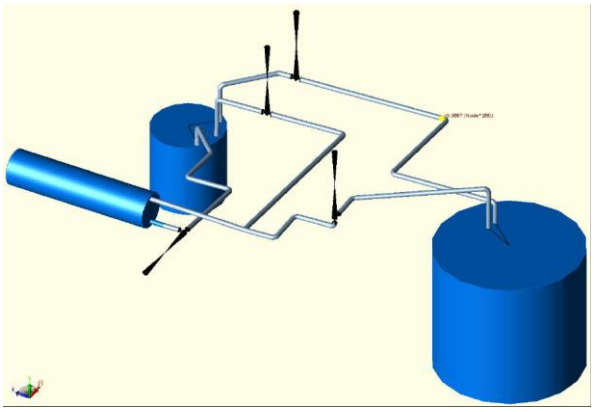

(c)

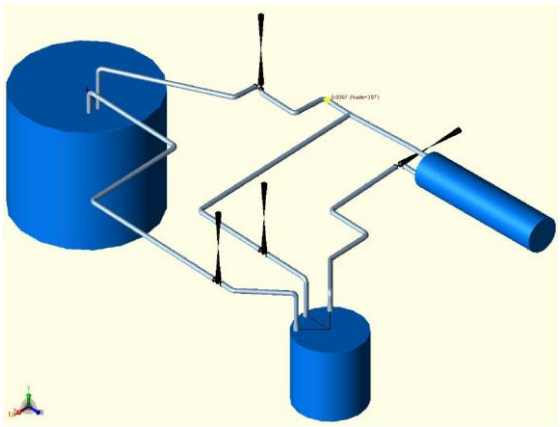

Figure 48: Maximum displacements: (a) 0.64" maximum in the +x direction (b) 0.57" in the -y direction (c) 0.90" in the –z direction .

5. Conclusions and Path Forward

All design work is nearing completion and construction of THETA primary and secondary sodium systems should begin in the coming months. Given the rigor of design work and safety analysis on the facility and the collaboration of designers with systems code developers, THETA will be an important asset for the METL facility and for sodium cooled reactor component and code development.

6. Acknowledgements

The authors would like to acknowledge the rest of the Mechanisms Engineering Test Loop (METL) team, Anthony Reavis and Daniel Andujar, for all of their hard work and dedication to constructing, maintaining and operating the facility. The authors would also like to acknowledge Dzmitry Harbaruk and Henry Belch for their assistance in monitoring METL systems during 24-hour operations. This work is funded by the U.S. Department of Energy Office of Nuclear Energy's Advanced Reactor Technologies program. A special acknowledgement of thanks goes to Mr. Thomas Sowinski, Fast Reactor Program Manager for the DOE-NE ART program and to Dr. Robert Hill, the National Technical Director for Fast Reactors for the DOE-NE ART program for their consistent support of the Mechanisms Engineering Test Facility and its associated experiments, including the Thermal Hydraulic Experimental Test Article (THETA). Prior years' support has also been provided by Mr. Thomas O'Connor, Ms. Alice Caponiti, and Mr. Brian Robinson of U.S. DOE's Office of Nuclear Energy.

7. References

[1] N. Tanaka, S. Moriya, S. Ushijima, T. Koga, and Y. Eguchi, "Prediction method for thermal stratification in a reactor vessel," *Nucl. Eng. Des.*, vol. 120, no. 2–3, pp. 395–402, 1990.

[2] Y. Ieda, I. Maekawa, T. Muramatsu, and S. Nakanishi, "Experimental and analytical studies of the thermal stratification phenomenon in the outlet plenum of fast breeder reactors," *Nucl. Eng. Des.*, vol. 120, no. 2–3, pp. 403–414, 1990.

[3] M. T. Weathered, "Characterization of Sodium Thermal Hydraulics with Optical Fiber Temperature Sensors," 2017.

[4] C. Grandy, H. Belch, T. Kente, and M. Weathered, "Letter Report of the Mechanism Engineering Test Loop (METL) Current Test Plan," 2018.

[5] Y. Chang, P. Finck, and C. Grandy, "Advanced Burner Test Reactor Preconceptual Design Report," 2006.

[6] J. K. Fink and L. Leibowitz, "Thermodynamic and Transport Properties of Sodium Liquid and Vapor," pp. 1–238, 1995.

[7] T. Sumner and A. Moisseytsev, "Simulations of the EBR-II Tests SHRT-17 and SHRT-45R," in *16th International Topical Meeting on Nuclear Reactor Thermal Hydraulics (NURETH-16)*, 2015.

[8] W. Logie, C. Asselineau, J. Pye, and J. Coventry, "Temperature and Heat Flux Distributions in Sodium Receiver Tubes," no. December, 2015.

[9] E. Skupinski, J. Tortel, and L. Vautrey, "Determination des coefficients de convection d'un alliage sodium-potassium dans un tube circulaire," *Int. J. Heat Mass Transf.*, vol. 8, no. 6, pp. 937–951, 1965.

[10] Maresca and Dwyer, "Heat Transfer to Mercury Flowing In-Line Through a Bundle of Circular Rods," *Trans. ASME*, 1964.

[11] Foust, *Sodium-NaK Engineering Handbook Vol II*. 1979.

[12] R. K. Sinnott, *Chemical Engineering Design*. Elsevier, 2005.

[13] "Flow of Fluids Through Valves, Fittings, and Pipe," NY, 1982.

[14] W. C. Gray and E. R. Astley, "Liquid Metal Magnetic Flowmeters," *J. Instrum. Soc. Am.*, 1954.

[15] H. G. Elrod and R. R. Fouse, "An Investigation of Electromagnetic Flowmeters," *Trans. Am. Soc. Mech. Eng.*, 1952.

[16] J. Liu, P. Vora, P. Dent, and M. Walmer, "THERMAL STABILITY AND RADIATION RESISTANCE OF SM-CO BASED PERMANENT MAGNETS," in *Proceedings of Space Nuclear Conference 2007*, 2007.

Nuclear Science and Engineering
Argonne National Laboratory
9700 South Cass Avenue, Bldg. 208
Argonne, IL 60439

www.anl.gov

Argonne National Laboratory is a U.S. Department of Energy laboratory managed by UChicago Argonne, LLC